EMPIRICAL CONFIRMATION OF THE MASS DEPENDENCE FOR WHITE DWARF LUMINOSITIES

JEREMY ROBERT WILSON BECKETT

A thesis submitted in partial fulfillment of the requirements for the degree of Master of Science

Saint Mary's University
Halifax, Nova Scotia
December 1993

ISBN 0-315-90953-6

Canada

The Examining Committee

Dr. D.G.Turner (Thesis Supervisor)
Professor of Astronomy and Physics
Saint Mary's University

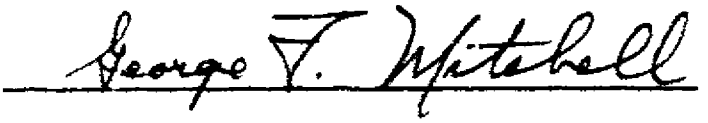

Dr. G.F. Mitchell
Professor of Astronomy and Physics
Saint Mary's University

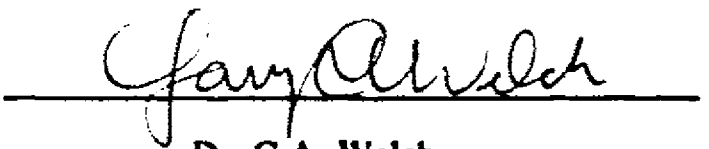

Dr. G.A. Welch
Associate Professor of Astronomy and Physics
Saint Mary's University

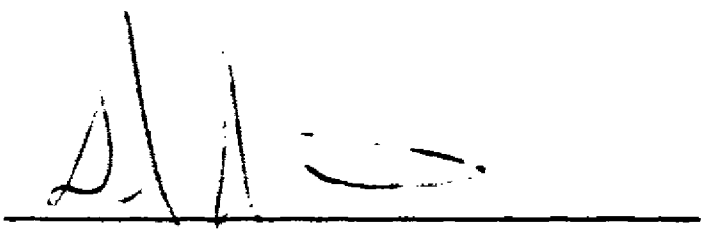

Dr. D.B. Guenther
Assistant Professor of Astronomy and Physics
Saint Mary's University

Abstract

Empirical Confirmation of the Mass Dependence
for White Dwarf Luminosities

Jeremy R.W. Becker December 1993

Existing calibrations of white dwarf luminosities have invariably relied upon the inhomogeneous sample of refractor parallaxes published in the General Catalogue of Trigonometric Parallaxes. We have completed a new calibration of white dwarf absolute magnitudes using a compilation of homogeneous and very accurate reflector parallaxes published by the U.S. Naval Observatory. The properties of the stars in this sample are well enough established that statistical luminosity corrections resulting from the combination of parallax errors with the space distribution peculiar to the stars can be established fairly reliably. The resulting luminosity calibration is in very good agreement with previously published results, and is of sufficient accuracy to investigate for the subset of DA-type stars the expected dependence on surface gravity (or mass) predicted theoretically from the white dwarf mass-radius relation. The results are in complete accord with expected results, which indicates that a full knowledge of the luminosity for any DA-type white dwarf requires information on its surface gravity as well as effective temperature. A byproduct of this study is a new estimate for the distance to the Hyades cluster, which contains several member DA stars.

Acknowledgements

I wish to thank all the people who have made the completing of my thesis possible, without whose support it would have been difficult, to say the least, to complete this thesis.

I wish to thank George Mitchell, for giving me the chance to study at Saint Mary's, and serving on my thesis defence committee. I would also like to thank Gary Welch for the same, and for the interesting classes I found it enjoyable to attend. Cameron Reed offered me employment at a financially critical time, and I thank Lori Reed for her kindness and useful advice. I wish also to thank David Guenther for serving on my defence committee, and providing numerous suggestions.

I wish to thank David Turner for being my thesis supervisor, and for his repeated explanations, and for having the patience to stay with a thesis project whose writing took considerably longer than either of us anticipated.

I wish to thank my parents, Judith and Malcolm, for insight, support and friendship, who made the doing of this thesis easier.

Lastly, but most importantly, I owe thanks to Jean Giannakopoulou, my closest friend, for her friendship and trust, without whom this thesis might not have seen an end. It is not accidental that science and the arts are allied as acts of creation. It should be remembered that in the end, both worlds are given meaning solely by the people who inhabit them.

Table of Contents

List of Illustrations

List of Tables

1. Introduction

The purpose of this thesis is to reexamine by empirical means the relationship between the temperature, luminosity and mass of a white dwarf that is predicted by theory.

The DA-type white dwarf stars form the primary subject of this thesis because, unlike other types of white dwarfs, the spectra of DA stars contain hydrogen absorption lines and continuum features which exhibit a strong gravity dependence even in broad band colour indices. The continua of other white dwarf types (e.g. DO) do not show such a dependence, making it difficult to establish their gravities by spectrophotometric means. It is possible to produce sophisticated stellar atmosphere models which predict the continuum colours one would expect to observe for a DA-type white dwarf of a given surface gravity (i.e. size) and effective temperature, as has been done for example by Koester et al. (1979). Effective temperatures inferred from the colours for DA white dwarfs can also be used to estimate bolometric corrections to their absolute visual magnitudes, under the assumption of course that such models are valid. The subsequent derivation of bolometric magnitudes for these stars requires reasonably correct absolute magnitudes, which are normally obtained using trigonometric parallax data.

White dwarfs were studied for a number of reasons. They are very common spatially (most stars should end their lives as white dwarfs) and, being structurally quite simple, can be modeled with somewhat greater ease than many other types of stars. They should occur in both open and globular clusters, but, being of exceedingly low luminosity, have been observed so far mostly in open clusters.

There are a number of steps involved in this thesis, and a brief explanation of these steps will be given in this introduction.

For various reasons it would be convenient to determine the relationship in terms of temperature, luminosity and radius of a white dwarf.

Luminosity depends directly on radius, according to

$$L = 4 \pi R^2 \sigma T_{eff}^4$$

$\pi = 3.1415927$

σ = Boltzmann's constant
T_{eff} = effective surface temperature
R = radius

Since luminosity can be measured geometrically, and effective temperature can be inferred from continuum colors matched to theoretical predictions from model atmospheres, it is possible to determine fairly directly the radius of a star. It is not possible to measure mass directly, save in the occasions when a white dwarf is a member of a binary system.

Fortunately the mass and radius of a degenerate star are directly related according to $R \sim M^{-1/3}$ (Cox & Giuli 1968, ch.25, for example). Furthermore, since surface gravity is another property of white dwarfs that can be inferred from continuum colours, it would be more convenient to relate surface gravity to luminosity:

$$g = \frac{GM}{R^2} \sim \frac{M}{R^2} \sim \frac{R^{-3}}{R^2} \sim R^{-5},$$

and, since luminosity

$$L = 4 \pi R^2 \sigma T_{eff}^4 \sim R^2 \text{ for } T_{eff} = \text{constant}$$

we have $g \sim L^{-5/2}$

or $$\log g \sim -\frac{5}{2} \log L \sim M_{bol}.$$

This luminosity, expressed as a bolometric magnitude, should show a linear dependence on the logarithm of the surface gravity, and this is ultimately what this thesis seeks to determine.

Determination of the luminosity, or the bolometric magnitude, of a star is dependent upon an accurate knowledge of its distance. The most direct method of estimating distances to stars is by means of their trigonometric parallaxes. Unfortunately, even the nearest stars are distant enough that they have very small parallaxes, so measuring errors tend to limit the reliability of distances obtained in this manner.

Systematic errors, often of unknown source, and uncertain corrections from relative to absolute parallax have combined to limit the precision of most older parallaxes to about ± 0".010 or ± 0".020. This situation has changed in recent years, however, with improvements in measuring techniques, and currently the smallest quoted uncertainties in ground–based parallaxes are those obtained in the United States Naval Observatory (USNO) surveys of nearby stars (Harrington & Dahn 1980; Dahn et al. 1982; Harrington et al. 1985; Dahn et al. 1988, etc.). The mean uncertainty in these lists (for white dwarfs) is ± 0".0037, which seems to represent the total mean error of a USNO parallax. This means that parallaxes smaller than 0".037 (corresponding to distances in excess of 27 parsecs) will suffer from relative errors in excess of 10%.

Furthermore, there is an added bias which creeps into Mv estimates due to parallax uncertainties themselves. See chapter 5, "Parallax Corrections", for a detailed explanation. Hanson (1979) developed a convenient means of correcting for this bias, using proper motion data, and this is also explained in chapter 5. With good Mv estimates, we can proceed to estimate M_{bol} for each star via the model atmospheres mentioned earlier.

Bolometric corrections (BC) are temperature-dependent. Using a model atmosphere template generated by Koester et al. (1979) we can determine a surface gravity and temperature which would reproduce the U-B, B-V colours we observe for any given star. Shipman (1972) and Wesemael et al. (1979) estimated $\log T_{eff}$-based bolometric corrections covering low (5000K-20 000K) and high (20 000K-100 000K) surface temperatures respectively. These data were combined to produce a BC relation which I fit with a third-degree polynomial. Knowing bolometric magnitudes (i.e. luminosities) it is possible to estimate the radius of each white dwarf using the standard radius-temperature-luminosity relation. These radii, combined with surface gravity estimates, permit the estimation of white dwarf masses. Using the mean of the logarithm of these radii, we can also determine if a luminosity-mass (i.e. surface gravity) relationship exists.

In order to detect any mass-dependence of luminosity, it was decided to calculate the bolometric magnitude each star would have if each had the same mean radius and subtract from each star its actual bolometric magnitude. The idea behind this is that if there is any systematic difference between the bolometric magnitudes of a set of stars all of identical radius ($^{R}M_{bol}$) and bolometric magnitudes of a set of stars each identical to its corresponding star in the first set in all properties but radius (M_{bol}) (i.e., each with its own radius), that systematic difference will be caused by radius. We are looking for a mass-dependence in luminosity, and the differences are plotted against surface gravity (this also being dependent on mass) rather than radius since surface gravity is directly inferred from UBV colours, while radius is inferred from surface gravity and temperature; it is one step further removed from direct observation. As this thesis shows, such a dependence on gravity (i.e radius, i.e mass) exists in a demonstrable way.

This relation allows an interesting way to estimate the distances to DA white dwarfs without having to determine trigonometric parallaxes. This is a side result of this thesis.

Once one has a relationship between luminosity, temperature, and mass, or equivalently a relationship between bolometric magnitude (from photometric observations and inferred temperatures), temperature (estimated from photometric observations), and surface gravity (estimated from photometric observations), one has a calibration curve that can be used to estimate the distances to white dwarfs via photometric observations.

The first step in this process is to use B-V, U-B data to produce log T_{eff} and log g estimates via the model atmosphere templates mentioned in this thesis. The gravity estimate of a star is applied to the bolometric magnitude-surface gravity calibration curve to obtain an estimated $^{R}M_{bol}$-M_{bol}, and the temperature estimate is used, along with the assumption that the mean radius determined for the stars in the main body of the sample is good for all nearby white dwarfs, to calculate $^{R}M_{bol}$. The difference between these two values provides an estimate for M_{bol}. We calculate and subtract the bolometric correction

from this value to obtain Mv, and this, along with V for a given star, provides an estimate of distance modulus. This is done for the Hyades cluster, using data taken from the Catalogue of White Dwarfs (Agayev, 1982), which is a compilation of available UBV, proper motion, and other data from various sources.

The techniques used in this thesis are based upon the use of trigonometric parallaxes from the USNO lists, and take account of well-known systematic bias inherent in trigonometric parallax data. The correction of such bias, a procedure not undertaken in previous white dwarf calibrations, adjusts the luminosities of all stars in our sample to their most likely correct values. This adjusted sample forms the basis of the present luminosity calibration.

2. White Dwarf Classification Schemes

The classification scheme currently in use for white dwarfs is both spectroscopic and photometric in nature, being based upon detailed data of both types (Sion et al. 1983). The identification symbols are composed of four parts. a) D for degenerate, b) an upper case letter signifying the primary spectroscopic feature in the spectrum; c) an upper case letter signifying any secondary spectral features, and d) a numerical temperature index ranging from 0 (the highest temperature) to 9, defined by:

Index = $10 \times \theta_{eff}$ = 50,400°K/T_{eff} (truncated — see explanation which follows).

Spectral features. The letter A is used to indicate the presence of hydrogen Balmer lines in the spectrum of the object, B to indicate He I absorption lines, C to denote a reasonably featureless spectrum with no absorption lines deeper than 5% of the continuum, and O to indicate the presence of He II (He I and/or hydrogen Balmer lines may also be present). The presence of metal lines is indicated by Z (this includes Ca I, Ca II, Fe I, N, and TiO, but no H or He lines), and Q denotes the presence of lines of either atomic or molecular carbon. For example, a white dwarf showing strong He I absorption lines with weak Ca II features would be classified DBZ, and a star with dominant He II and weak N V (in the ultraviolet) would be designated DOZ. Non-optical spectral components will, in the case of DQ stars, be included as primary spectral features, but in all other classes as secondary features only.

The temperature index is truncated to an integer, and is based upon the availability of reliable effective temperatures for white dwarfs. It is used in the following way. A star of effective temperature 30,000°K would be designated with the index 50,400/30,000 = 1.68, truncated to 1, while a star of effective temperature 8,000°K would be designated with the index 50,400/8,000 = 6.3, truncated to 6. All stars with effective temperatures cooler than 5,500°K receive the index 9.

An older classification system (Greenstein 1960) is used in most earlier references (e.g. Graham 1972), and will be explained briefly. The primary classification symbol in this scheme is still D. The spectral symbols (of which there is only one per star) are as follows: A stands for hydrogen Balmer absorption, B denotes strong He I lines, C indicates a continuous spectrum with no absorption features deeper than 10% of the continuum, A.F (the only compound symbol) indicates sharper but weaker Balmer lines plus weak Ca II features, F indicates that Ca II and Fe I are present but that there is no hydrogen seen, K is used to indicate the presence of weak Ca II lines with no other features, M is used for those objects where Ca II is strong but Ca I is weak (there may also be TiO lines seen), O denotes the presence of strong He II lines with weaker He I and/or Balmer secondary features, λ4135 is used to designate those objects with unidentified "Minkowski" bands, λ4670 identifies objects exhibiting broad bands at λλ4670 and 5165, and C_2 is interchangeable with the λ4670 designation (both indicate the probable presence of molecular carbon). There are additional subclassifications for polarization and line strength features: p implies the existence of peculiar lines, P that there have been measurements of strong polarization in the object, wk indicates that the strongest lines are quite weak, e indicates the presence of emission features, s denotes sharp lines, ss very sharp lines, n diffuse lines, and PEC peculiar lines.

The older nomenclature system was superseded with improvements in photometric observations, as it became apparent that some older stellar classes arose as a result of misidentification of spectral features. For example, the designation DK no longer applies to any particular star.

3. White Dwarf Parameters from Photometry

A Brief Discussion of the UBV log g, T_{eff} Conversion.

In order to gain some understanding of the physical state of white dwarfs, it is important to have some idea of the sizes, masses, and temperatures of these stars. The only direct measurements we can make are photometric, spectroscopic, and positional measurements. Photometry gives information about how much energy the white dwarf emits at various wavelengths, while spectroscopic observations give information on the chemical composition of the stellar surface layers. Positional measurements provide important data on the parallaxes and proper motions of these stars, and in a few instances of orbital motion around a companion.

Because luminosity is dependent on both size and temperature, we need some means of determining both the radius and temperature to completely specify a star. Temperature is generally the easier of the two to determine.

The best method for determining temperatures for white dwarfs is by using model atmospheres of specified chemical composition, effective temperature, and gravity as a means of matching the observable stellar continua and line profiles. Colour-colour data can be matched to model atmosphere predictions if one is not concerned about high accuracy, and this is what this thesis proposes to do.

Chemical composition is an important parameter in this method. Current observations suggest that the range of H and He abundances in the atmospheres of white dwarfs is greater than in "normal" non-degenerate stars, but even large variations in H and He abundance do not seem to affect broad band colours by a significant amount, at least for DA types.

The reason we use DA white dwarfs in this thesis is that these are the only class of white dwarf with continuum features that show some sort of gravity-dependence.

Furthermore, it is easier to solve for the effective temperatures of DA stars than for non-DA stars because the former show a quite simple hydrogen spectrum. This makes it possible to include line-blanketing effects in their model atmospheres in a simple fashion. With helium-dominated or more complex atmospheres, so many more absorption lines are involved for both the neutral and ionized atoms that modelling becomes more complex.

What is new about my thesis, and what makes the doing of it worthwhile, is the homogeneity of the data set; all the proper motion and parallax data are from the tables of the USNO parallax star lists. These data are clearly incomplete for small proper motions or for bright stars. In the first case this arises as a result of the difficulty of detecting small proper motions, and in the latter case the problem is due to the inability of the instruments at the USNO to measure parallaxes for bright stars. The latter is not a problem for white dwarfs. However, the USNO lists are extensive and represent the most comprehensive and accurate source of white dwarf parallaxes to date, at least until the HIPPARCOS mission begins to generate data. There is also the advantage that the data were obtained in a homogeneous fashion. Thus, any systematic bias in the data should be uniformly applied across the sample, which would probably not be the case were the data collected by different methods. Additionally, the accuracy of the data is exceedingly good for ground-based parallaxes. According to the USNO staff, the uncertainty in matching their fine-grain photographic plates to the true FK4 system is $\approx \pm 0.002$ arcsec. This is also their estimate of their internal, measuring accuracy. Thus, the uncertainties in parallax measurement they report seem to represent the true external errors. Such has not been the case for the sample of white dwarfs in the General Catalogue of Trigonometric Stellar Parallaxes (GCTSP) which was used in previous calibrations of white dwarf luminosities.

4. The White Dwarf Sample

The most accurate parallax data available to-date are the faint star parallaxes compiled by the USNO. A computer was used to calculate the correction to the absolute visual magnitude, ΔM for the white dwarfs in this sample. Position and proper motion data were taken from Tables 2 and 3 and the n-values 0.1, 1.8, and 2.6 were obtained from the three best-fit slopes of the log $N(\mu)$-log μ plot in Figures 2 to 4. Each n-value applies over a particular range of proper motion, and each star whose proper motion places it in a certain μ-range had its luminosity adjusted using the relevant exponent n. The results, in the format: epsilon, original absolute magnitude, uncertainty, absolute magnitude adjustment, and final adjusted absolute magnitude and uncertainty, are listed in Table 4 for every star in the sample. See page 16 for further explanation. The uncertainty of the adjustments is not listed, but is sometimes larger than the original absolute magnitude uncertainty so that its effect on the total uncertainty in absolute magnitude is quite marked.

5. Parallax Corrections

The effects of luminosity bias when using a sample of stars of measured trigonometric parallax, π, are reasonably well–established. As has been pointed out by Trumpler and Weaver (1953), for example, any selection of stars by a lower limit in parallax (either implicit or sample–dependent) will result in an excess of stars with systematically large parallaxes in the sample. The problem is commonplace, and arises because of the inevitable measuring uncertainties in trigonometric parallaxes. Any parallax measurement π_o has an associated uncertainty $\delta\pi_o$, which represents the standard deviation of the Gaussian error distribution of the observed parallax π_o about the true parallax π. A star with this measured parallax can therefore be pictured as lying on the surface of a shell of radius $r_o = 1/\pi_o$, with its true distance lying somewhere within the interval covered by the associated error limits $r_o + \delta r_o$ and $r_o - \delta r_o$, where $|\delta r_o| = \frac{\delta\pi_o}{\pi_o} \times r_o$. Potentially any point lying within the interval covered by these outer and inner limits could represent the true distance of the star of parallax π_o.

The corresponding distribution of the true parallaxes π about π_o for stars of observed parallax π_o is somewhat different, however, since it is skewed relative to π_o due to the manner in which stars are distributed in space. The spatial volume covered by a shell with distance limits of r_o and $r_o + \delta r_o$ is clearly larger than one with distance limits of r_o and $r_o - \delta r_o$, so that for most types of stellar space distributions considered with respect to these shells there will always be more stars located in the outer portion of the error shell than in the inner portion. If the star with observed parallax π_o is one which has been selected at random from a parent population which is more–or–less uniformly distributed within this error shell over the distance interval $r_o - \delta r_o$ to $r_o + \delta r_o$, then the average distance $\langle r \rangle$ of stars in this population must be greater than r_o. In other words, the distribution of true parallaxes π about the observed parallax π_o deviates from a Gaussian

shape, and reaches a maximum for $\pi < \pi_o$, depending critically upon the magnitude of the relative uncertainties in parallax as well as the actual space density of stars with measured parallaxes.

It is possible to correct for parallax bias when deriving absolute magnitudes for stars with measured parallaxes by taking into consideration both the observed parallax values, π_o, and their associated uncertainties, $\delta\pi_o$, relative to some assumed space distribution of the stars in the sample, as first suggested by Lutz & Kelker (1973). A more sophisticated approach has been adopted by Hanson (1979), who has devised a method which uses proper motion data to establish the probable space density distribution of the sample, which can then be used to correct for parallax bias. This method assumes that a simple power law describes the spatial distribution of a parallax sample, which is probably a valid approximation.

In the case of a constant space density of stars, $\rho \sim r^3$, a simple power-law distribution of the form;

$$F(r) = 4 \text{ pi } r^2 \rho \, dr ,$$

transforms (via $r = \pi^{-1}$, $dr = \pi^{-2} d\pi$) into a power-law distribution of parallaxes of the form;

$$P(\pi) = 4 \text{ pi } \rho \, \pi^{-4} \, d\pi .$$

The distribution of proper motions for these same stars should also be a simple power law of identical exponent since $\mu \sim \pi$, if the tangential velocities of the stars are comparable (Recall: $v_t = 4.74\mu/\pi$). If the space density distribution ρ of stars is non-uniform, the parallax distribution can at least be approximated by a power law of related form, namely:

$$P(\pi) = 4 \text{ pi } \rho \, \pi^{-n} \, d\pi ,$$

where n is the exponent of the distribution (= 4 for a constant space density). The comparable power law distribution for the proper motions will have the form:

$$N'(\mu) = K' \mu^{-n} \, d\mu .$$

The number of stars with proper motion greater than μ is readily evaluated, and is:

$$N(\mu) = \int_{\mu}^{\infty} N'(\mu)\, d\mu = \int_{\mu}^{\infty} K' \mu^{-n}\, d\mu = K \mu^{-(n-1)} = K \mu^{-x} .$$

The exponent $x = n+1$ for the distribution can be determined using a plot of log $N(\mu)$ versus log μ for stars in the sample (see Figure 2). If the sample's space distribution can be described satisfactorily by a power law, the data will tend to fall along a straight line of slope x, with typical values falling between 0 and 3 (where 3 represents a sample of constant space density).

As will be seen later, the space distribution for a sample of parallax stars is often characterized by non–integral exponents x. Such values are of dubious physical significance, however. Over the small distances involved for the white dwarfs in our sample, it seems likely that any deviation from $n = 3$ (which describes a constant space density) is due to sample incompleteness.

All of the USNO compilations for their parallax program include accurate positional data (coordinates, proper motions, and parallaxes) as well as new photoelectric photometry for each star. The latter are used to generate absolute visual magnitudes, M_V, for each star, which, in combination with B–V colour indices, can be used to identify white dwarfs in the sample (see Figure 1). It is therefore a relatively simple matter to extract all of the white dwarfs from the USNO lists, as we have done here. The proper motion data are of immediate interest for determining the space distribution characteristics of the sample, so a partial listing of these data are given here.

The data for our present sample have been arranged into bins of decreasing proper motion containing five stars each, except for the last (and smallest proper motion) stars. For simplicity, the star with the smallest proper motion in each bin is then used to specify μ in the calculation of $N(\mu)$. Other binning schemes were tried, such as grouping 6, 7, 8, 9, or 10 stars per bin, or grouping the stars per 0".10 of proper motion, but the method adopted here seemed to provide the most convenient straight–line fit at the final fitting stage. The data are presented in Table 1, and are plotted in Figure 2.

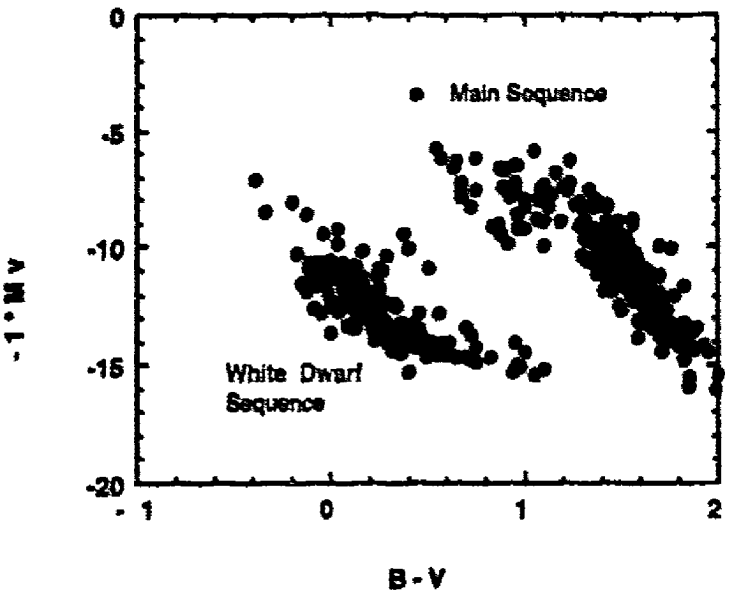

Figure 1. Colour–magnitude diagram for all stars in the USNO sample, showing the distinction between the main sequence and the white dwarf region.

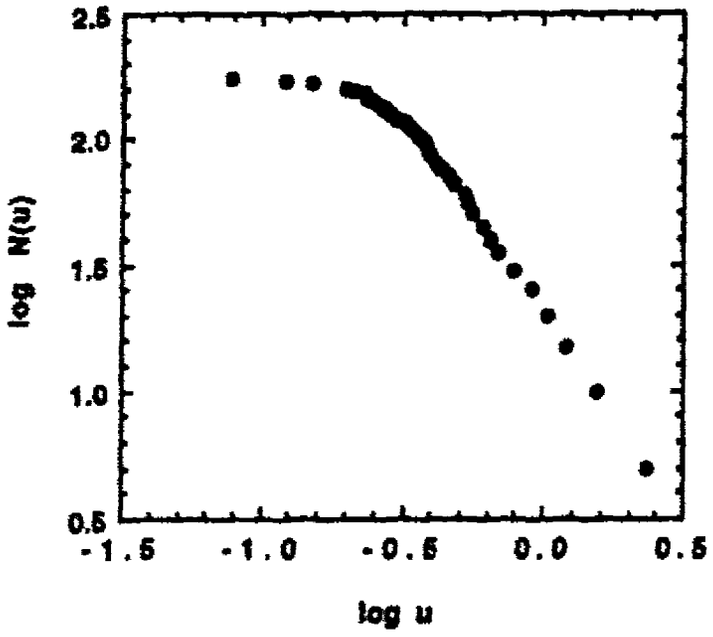

Figure 2. A plot of log μ - log N(μ) for the binned data sample, where N(μ) is the number of stars with proper motions greater than or equal to μ. It demonstrates the power law relationship described in the text; the curvature of the relation indicates different levels of sample completeness.

It is evident that the data are not satisfied by a relation having a single exponent x. They can, however, be approximated well by three separate straight lines of differing slope over different μ intervals. The variation of x with μ actually traces the differing levels of completeness of stars in the USNO program. High proper motion stars are most completely represented in this program, presumably because these stars are readily detected in proper motion surveys. Stars of small proper motion are not well represented, however, so the power law distribution for program stars of small μ deviates progressively further from a constant space density distribution as the μ-limit decreases.

In an attempt to ensure impartiality when analyzing the data of Figure 1, the proper motion limits for the various subsamples were determined by the following procedure. Starting at the high-proper motion end of Figure 2, the slope x of the fitting relation was calculated using only the data for stars in the first two bins, then using the data for stars in the first three bins, the first four bins, and so on, until every bin was included in the slope. Obviously, a single straight line of unique slope would provide a very poor fit for all of the data points in Figure 2, although the fits for the binned data should yield nearly constant slopes for that range of data points which are satisfied by a power law of common slope. A plot of the calculated slopes relative to the number of bins involved is presented in Figure 3, where it can be seen that a power law of slope $x = -1.6$ provides a fairly good description for all of the data in bins 1 to 23. At that point the data diverge noticeably from a power law of this slope. Figure 4 shows the rest of the data, the less-complete range. This cumulative-slope plot shows that another single power-law fits well the next eight bins, leaving the last five bins by themselves. For those ranges over which the slope remains relatively constant, we may apply the mean slope calculated for that range as the representative value of the exponent x for the group. At the low proper motion end of the log N(μ) versus log (μ) plot in Figure 2, we find that the five leftmost bins are well fit by a nearly horizontal line of slope $x = -0.1$, while we can fit the middle seven bins by another straight line of slope $x = -0.8$. The actual best-fitting relations for

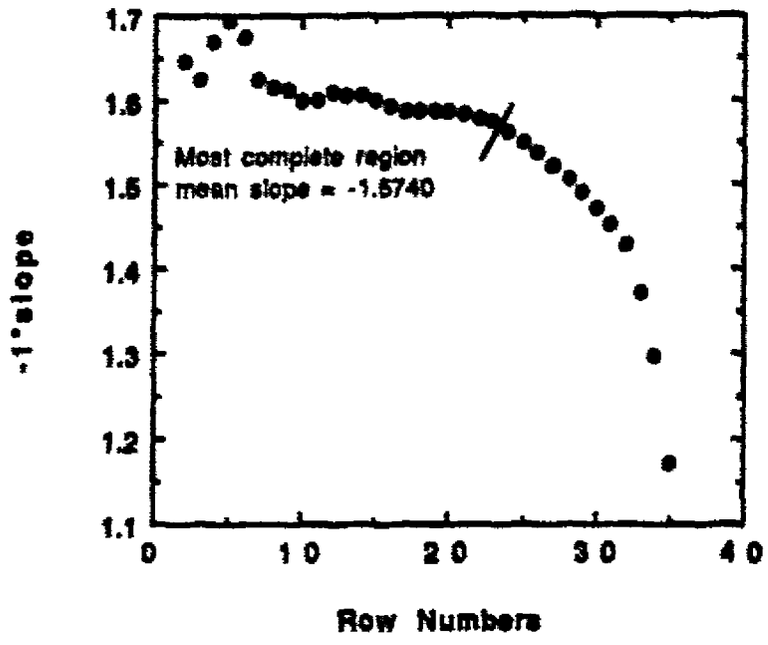

Figure 3. Plot of the cumulative slope (per x number of bins) versus the number of bins of data included in the slope calculation. The cutting line marks where the slope of the accumulated points begins to diverge markedly from the accumulated mean. This point we took to indicate the limiting range over which a power law could be applied to the data.

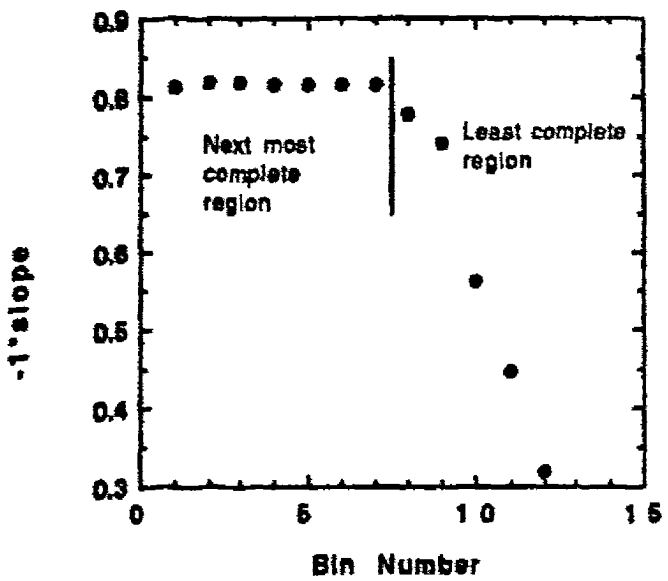

Figure 4. Plot of cumulative slope versus bin number for next and least-complete regions. The cutting line indicates the limiting ranges for the adopted power law fits to the data.

the high proper motion section of the sample ($\log \mu \geq -0.45$), the middle section of the sample ($-0.45 > \log \mu \geq -0.67$), and the low proper motion section of the sample ($\log \mu < -0.67$) are depicted in Figure 5, and have slopes of -1.5740 ± 0.0138, -0.8175 ± 0.0105, and -0.1321 ± 0.0095, respectively. However, it is unnecessary to adopt such precise values for the parameter x when it is not clear how accurately they represent the true space distributions of sample stars.

The parameter x yields an exponent n, via $n = 1-x$ (see Hanson 1979), which is used as the power law exponent in the subsequent absolute magnitude corrections.

For a power law exponent n, the correction for bias in absolute magnitudes derived from parallax data is inferred by Hanson (1979) to be described by the relationship:

$$\Delta M = 2.17\left[\frac{A_2\varepsilon^2 + 3A_4\varepsilon^4}{1 + B_2\varepsilon^2 + B_4\varepsilon^4}\right], \qquad (1)$$

with an uncertainty of roughly:

$$\Delta(\Delta M) \approx \pm |2A\varepsilon + 3B\varepsilon^3|\,\Delta\varepsilon\,, \qquad (2)$$

where

$$A_2 = -(n+0.5)$$
$$A_4 = -\left(\frac{1}{4} + \frac{n}{3} + \frac{n(n+1)}{4} + \frac{n(n+1)(n+2)}{6}\right)$$
$$B_2 = \frac{n(n+1)}{2}$$
$$B_4 = \frac{n(n+1)(n+2)(n+3)}{24}$$
$$A = -2.17(n+0.5)$$
$$B = -2.17\left(\frac{6n^2 + 10n + 3}{4}\right).$$

$\varepsilon = \delta\pi/\pi_o$ is the relative uncertainty in the observed parallax, and $\Delta\varepsilon$ is the uncertainty in the relative error — approximately 4ε according to Hanson (1979).

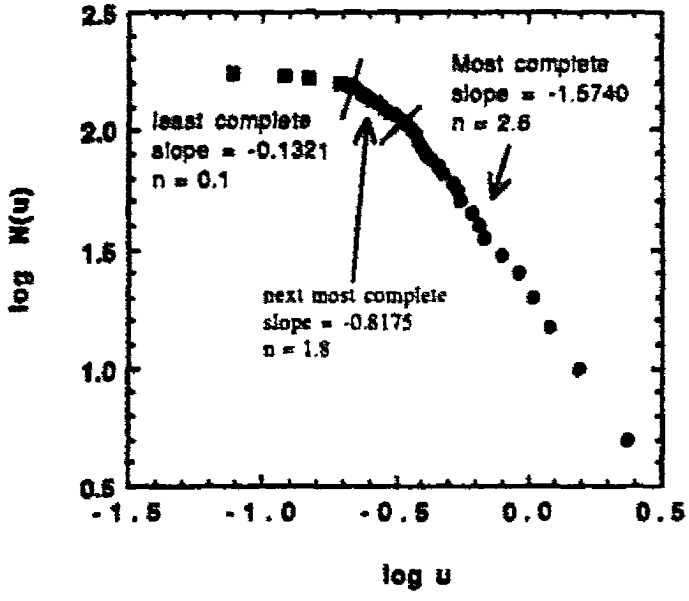

Figure 5. Plot of log(μ) versus logN(μ), showing the range of proper motions over which a power law of constant slope can be assumed to fit the data. The regions were determined by the data of figures 2 and 3.

6. Application of Theory to Main Sample

The first step in the analysis is the correction of the absolute visual magnitudes, using the equations (1) and (2). As an example, we find sample corrections for stars with $\log \mu \geq -0.45$ as follows:

For this group, $n = 2.6$

$A_2 = -3.10$

$A_4 = -10.6327$

$B_2 = 4.68$

$B_4 = 10.0464$

$A = -6.727$

$B = -37.7363$

Thus, in the case of star W1 in Tables 2, 3, 4:

$$\varepsilon = \frac{0.0048''}{0.0337''} = 0.1424$$

$$\Delta\varepsilon = 4\varepsilon = 0.5696$$

Therefore $\Delta M = 2.17x\dfrac{-3.10x(0.1424^2) + 3x(-10.6327)(0.1424^4)}{1+4.68x(0.1424^2) + 10.0464x(0.1424^4)} = -0.1490,$

and the uncertainty in the correction is

$$\delta(\Delta M) = |2x(-6.727)(0.1424) - 3x(37.7363)(0.1424^3)| \times 0.5696 = \pm 1.2775$$

The adjusted absolute magnitude for W1 is thus

$$M_V(\text{corr}) = M_V(\text{uncorr}) + \Delta M = 12.98 + (-0.1490) = 12.83$$

with an uncertainty of

$$\delta M_V(\text{corr}) = \sqrt{\delta M(\text{uncorr})^2 + \delta(\Delta M)^2} = \sqrt{0.13^2 + 1.2775^2} = \pm 1.28$$

It was necessary to eliminate from the sample known non–DA stars and those stars whose ε–values are larger than ε_{max} for a particular μ–range. This last step eliminates stars for which the ratio of parallax error to observed parallax is so great that the magnitude corrections derived from Hanson's (1979) method cannot be assumed to be accurate (i.e. their relative adjustments are too great). The objects are listed in Table 6. As may be seen from Table 6, the relative uncertainties for these stars are up to 650% of the primary value, so they can be reasonably excluded from the sample.

Non–DA stars are identified from their spectral classifications by Graham (1972) and Wegner (1979, 1984) on the basis of spectroscopic appearance. In cases where authors disagreed, I assumed the most recent classification was correct.

To prune the sample further we need the effective temperature of each star. The effective temperature and surface gravity of each DA star was derived by fitting the USNO colour–colour data to the UBV template (Figure 6) constructed by Koester et al. (1979). De-reddening was not necessary because these stars are sufficiently close that reddening is not significant. When this was done, 76 stars remained in our lists (Table 7). The other stars were excluded not necessarily because they are non–DA, but simply because they did not fit the range of the template (and thus no temperature and surface gravity could be established), or because the USNO data lacked a U–B colour. To get some idea of the accuracy of our temperature and gravity estimates, we make use of the estimates calculated by Bergeron et al. (1992) from fitting hydrogen line profiles to the estimates of new, more accurate model atmospheres. The data show, for such stars as we have in common, that our temperature estimates differ from Bergeron et al.'s by 6.5% or less in all but one case, and our log g estimates by 5.8% or less in all but one case, for the same star, He 3 (Table 8). Our temperature estimates are, however, higher than those of Bergeron et al. save for two stars, and our log g estimates are lower than those of Bergeron et al. save for one star. These differences are included in Table 8. The small differences suggest to us that our data are trustworthy, but the differences might result in systematic differences later on.

We now calculate the bolometric correction to each star's absolute visual magnitude.

The bolometric correction scales adopted here are from Liebert et al. (1988), as compiled by Shipman (1972) and Wesemael et al. (1980) (see Table 9 and Figure 7).

The fitting relationship is

$$B.C. = -190.02 + 126.95 \times \log_{10}(T_{eff}) - 27.254 \times [\log_{10}(T_{eff})]^2 + 1.8382 \times [\log_{10}(T_{eff})]^3$$

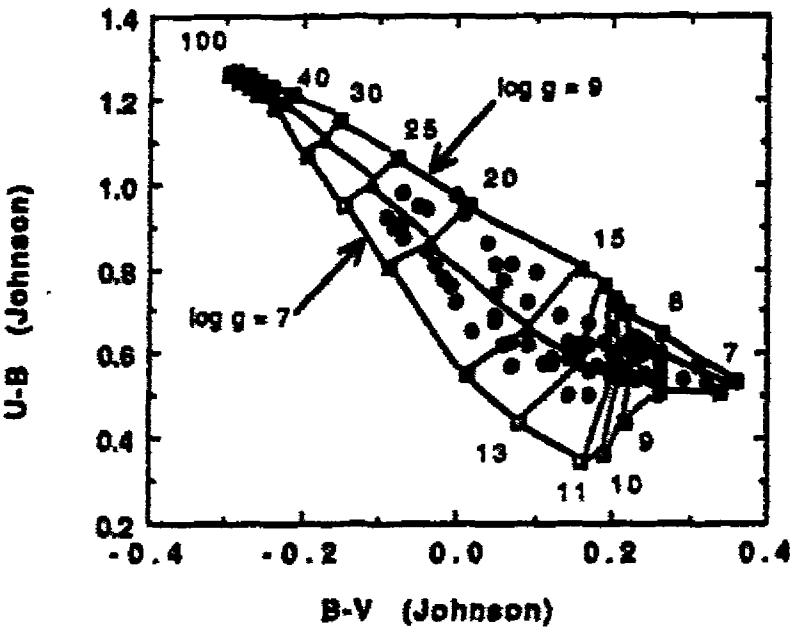

Figure 6. Temperature–log g template from Koester et al. (1979) The lines with positive slope in the plot are isotherms, the lines with negative slope are isogravs, and the dark circles are the B–V and U–B data for stars which fall in the template region. Temperatures in 1000 K units are 100, 75, 60, 50, 40, 30, 25, 20, 15, 13, 11, 10, 9, 8, 7. Gravity lines are log(g) = 7, 8 and 9.

As an example, a sample correction is applied to W672A, which has an inferred effective temperature of 13,970 ± 230 °K:

$$M_{bol} = M_V + B.C.(T_{eff} = 13970)$$
$$= 11.09 + (-1.18)$$
$$= 9.91$$

The corresponding uncertainty in the bolometric correction (see Bevington, 1969) is

$$\Delta B.C. = \sqrt{(1*0.01/4.15)^2+(2*0.01/4.15)^2+(3*0.01/4.15)^2}$$
$$= 0.01$$

So, the bolometric correction for W672A is -1.18 ± 0.01, and the corresponding bolometric magnitude of W672A is

$$M_{bol} = M_V+B.C. \pm \sqrt{\Delta M_V^2+\Delta B.C.^2}$$
$$= 9.91 \pm 0.39$$

The uncertainty in the bolometric corrections are thus quite small, and will not greatly affect the uncertainties in bolometric magnitude. See Table 10.

Estimated errors in our temperatures and gravities were calculated by assuming a mean error in B–V and U–B of ±0.02 magnitude, as determined from the USNO data, and finding corresponding variations in log g and T_{eff}.

We checked the sample for problems of completeness by plotting M_{bol}* versus log g in Figure 8. If, as this thesis seeks to demonstrate, luminosity is dependent on surface gravity, then an incomplete part of the sample should exhibit transformation problems via a large scatter when M_{bol}* is plotted against log g. The data were grouped according to temperature, around log T_{eff} of 3.90, 4.00, 4.10, 4.20, and 4.30, and each temperature group was fit by naked eye with a slope of –1, that predicted by theory. When this was done, the scatter in the low-temperature data convinced us that they should be discarded. Furthermore, we discarded seven other stars from the sample because they also showed excessive scatter or, as in the case of Feige 24, were double stars. 52 stars remained in the sample after this.

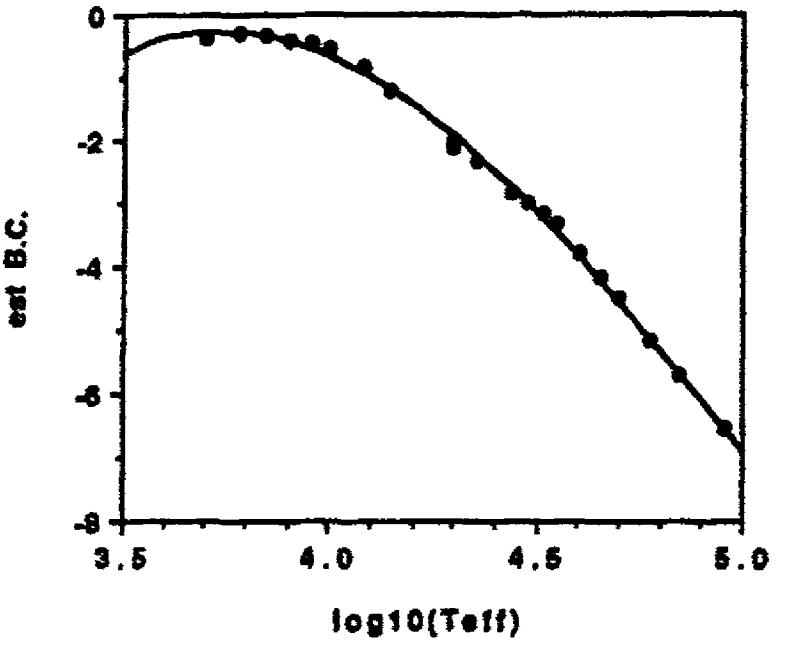

Figure 7; Plot of bolometric correction versus temperature for the combined Shipman-Wesemael et al. values; third order fit.

To verify that we effectively pruned the sample, we plotted M_{bol^*} versus log T_{eff} (see Figure 9).

This last diagram will help to weed out the remaining non-DA stars. The idea behind this is that, since the temperature-log g template (Fig. 8) was calculated for DA atmospheres all true DA stars analyzed should generate a relatively coherent temperature-bolometric magnitude (i.e. luminosity) plot, reflecting the idea that, as it cools, a white dwarf dims and cools smoothly without discontinuous jumps. Non-DA stars, showing only a weak gravity dependence in their spectral lines, will only fall into the UBV log g log Teff by accident and should not transform smoothly onto the temperature-luminosity plot. They can thus be distinguished from DA stars with some discrimination. It is evident that all remaining stars lie within a nicely-defined band and thus need not be eliminated from the sample.

The mean stellar radius of the white dwarf sample is estimated the following way. By this stage in the data reduction we know the temperatures of our sample stars and have an estimate of their bolometric magnitudes. From this we use the relationship for luminosity;

$$\frac{L_*}{L_\odot} = \frac{4\pi R_*^2 \sigma T_{eff}^4}{4\pi R_\odot^2 \sigma T_\odot^4}$$

σ=Boltzmann's constant

and note that

$$M_{bol(\odot)} - M_{bol^*} = 2.5 \log\left(\frac{L_*}{L_\odot}\right).$$

$$= 5 \log\left(\frac{R_*}{R_\odot}\right) + 10 \log(T_{eff^*}) - 10 \log(T_{eff(\odot)})$$

$M_{bol(\odot)} = 4.75$
$T_{eff(\odot)} = 5770$ K
M_{bol^*} = bolometric magnitude

so

$$M_{bol^*} = 42.36 - 5 \log\left(\frac{R_*}{R_\odot}\right) - 10 \log(T_{eff^*}) \quad (3)$$

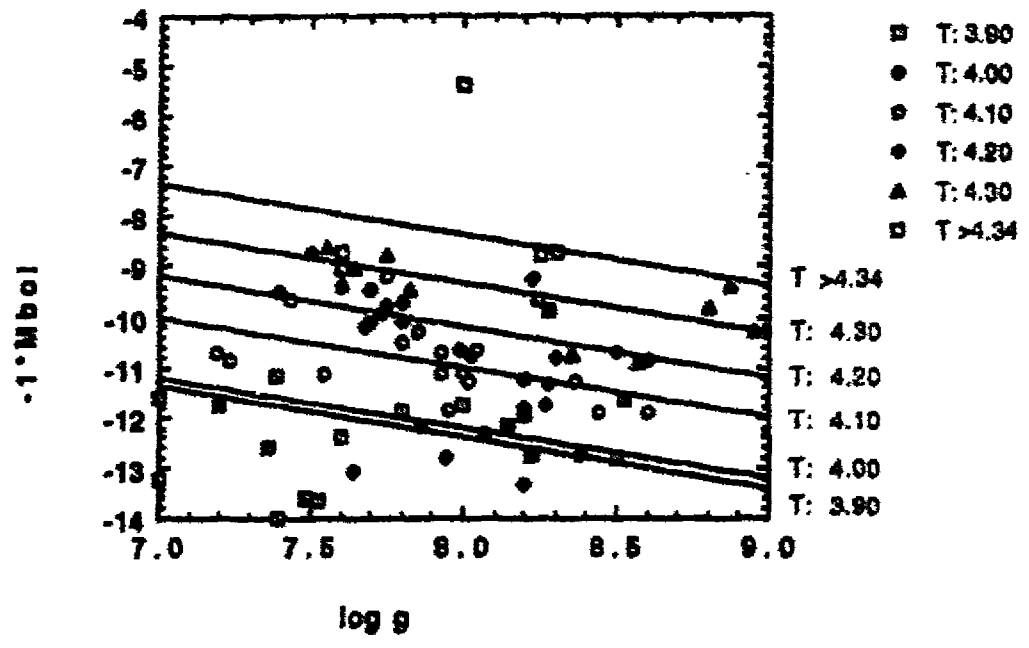

Figure 8. M_{bol} vs. log g for the remaining sample. The data are grouped by log Teff in units of 0.10, around 3.90, 4.00, 4.10, 4.20, and 4.30. All lines are fit by naked eye with a slope of –1, predicted by theory. The scatter for the low-temperature data, indicated by a , convince me that they are untrustworthy, and I exclude them and seven other stars for reasons of excessive scatter, or because, as in the case of Feige 24, they are actually binaries. Following this, 52 stars remain.

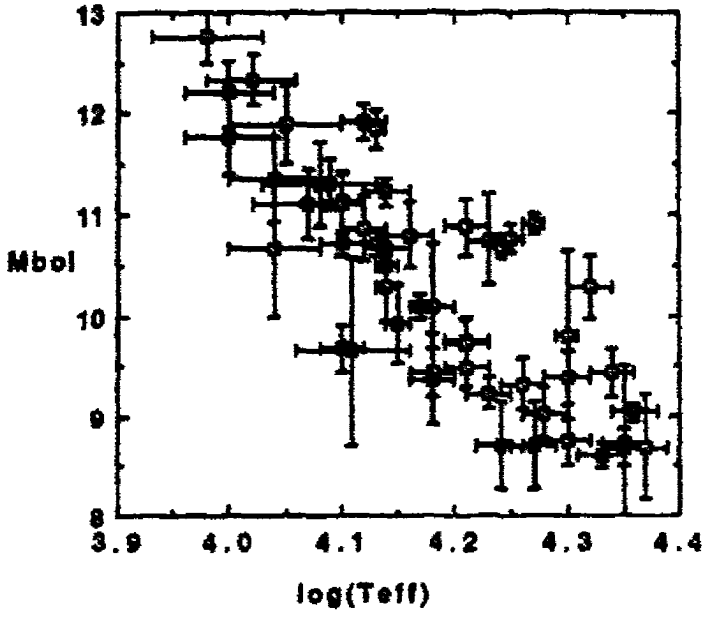

Figure 9. Plot of M_{bol} versus $\log T_{eff}$ for USNO sample. The data, with error bars, show that all the stars featured in the plot fall within a well-defined lozenge-shape, and that there are no 'stragglers' falling outside the main body. This means that all the stars *remaining* in the sample are probably DA-type.

The unknown in this equation is $\log\left(\frac{R_*}{R_\odot}\right)$, and the variable we use to find it is $\log(T_{eff*})$.

We can reduce this to a simpler form for a sample of N stars,

$M_{bol*_i} = A_i - 10 \log(T_{eff*_i})$, where −10 is the slope of the relation.

We solve for the mean intercept, <A>, by

$$<A> = \frac{1}{N} \sum_{i=1}^{N} [M_{bol*_i} + 10 \log(T_{eff*_i})].$$

The uncertainty in the intercept is given by

$$s_A = \frac{1}{N-1} \sum_{i=1}^{N} [A_i - <A>]^2,$$

and

$$\log\left(\frac{R_*}{R_\odot}\right) = 0.2(42.36 - <A>),$$

with uncertainty $\sigma = 0.2 s_A$

By this procedure, we find $\log\left(\frac{R_*}{R_\odot}\right) = -1.91 \pm 0.17$, or,

$<R_*> \cong 0.012\ R_\odot \cong 8600$ km radius.

Figure 10 displays the M_{bol*}–log (T_{eff}) relationship with lines of constant radius (the mean radius and the extremes from its standard deviation).

Using this radius, we recalculate the normalized bolometric magnitude (now called ${}^{R}M_{bol*}$ for constant radius) using equation (3) for each star and plot ${}^{R}M_{bol*}$–M_{bol*} versus log g (Figure 11). The relationship is

${}^{R}M_{bol*} - M_{bol*} = 7.227(\pm 1.504) - 0.933(\pm 0.188)*(\log g)$, with correlation coefficient $r = 0.574$. The result shows that luminosity decreases with increasing surface gravity, and therefore with increasing mass, as predicted. It also shows that the slope of the relationship of luminosity to gravity is, within uncertainties, equal to −1. To the knowledge of the author, this is the first time empirical confirmation of this predicted slope has been demonstrated.

Once the radius of each star has been determined, it is possible to estimate the mass of each star using the simple equation: $g = \frac{GM}{R^2}$. g = surface gravity of star.

G = Gravitational Constant
R = Radius of star.

We can express the mass of a star in terms of its radius and surface gravity, in terms of solar units, as

$\frac{M_*}{M_\odot} = \frac{g_*}{g_\odot}(\frac{R_*}{R_\odot})^2$, or as a logarithm.

$\log_{10}(\frac{M_*}{M_\odot}) = \log_{10}(g_*) + 2\log_{10}(\frac{R_*}{R_\odot}) - \log_{10}(g_\odot)$. $\log_{10}(g_\odot) = 4.44$.

As an example, we calculate the mass for W672A;

$\log_{10}(\frac{M_*}{M_\odot}) = 7.73 + 2x(-1.80) - 4.44$

$= -0.31$. This yields a mass ratio of $\frac{M_*}{M_\odot} = 0.49$. The mass ratios are listed in Table 11, along with log radii. Three of the stars in the sample have derived masses exceeding the Chandrashekhar limit of $\frac{M_*}{M_\odot} = 1.44$. When these anomalies are removed, the mean mass of the sample is 0.50 ± 0.33, lower than the mean mass found by Bergeron et al. (1992) of $\frac{M_*}{M_\odot} = 0.562 \pm 0.137$, but with a much larger scatter. This scatter may be due to several things. Since our data are broad band in nature, they are more likely to suffer contamination from extraneous light than the narrow band photometry used by Bergeron et al., resulting in generally less accurate estimates. The assumption that a mean mass may be applied to the sample used in this thesis may be unjustified, and lead to an incorrect M_{bol}- log g calibration. Additionally, there are many steps in our derivation of the white dwarf masses, providing many opportunities for errors to multiply. The mass estimates of Bergeron et al. were derived from the work of Wood (1990), whose equations were not stated. It is therefore not possible to make estimates of how the errors of Bergeron et al. were derived. However, the small scatter in their data may be a result of their mass estimate algorithm.

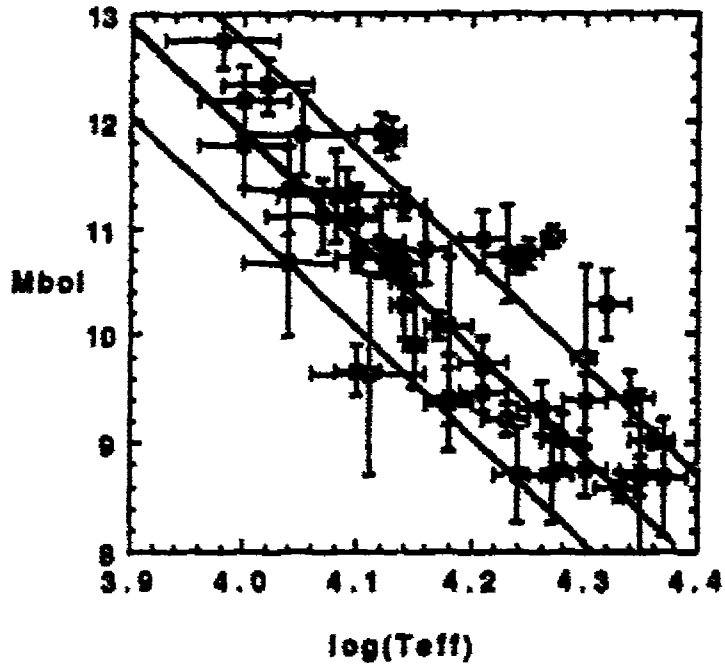

Figure 10. Variation of bolometric magnitude with temperature for the DA white dwarfs in the sample. The mean radius of $\log\left(\frac{R_*}{R_\odot}\right)$ = -1.91 and its limits of ± 0.17 are shown by the three lines. The data are the same as in Figure 9.

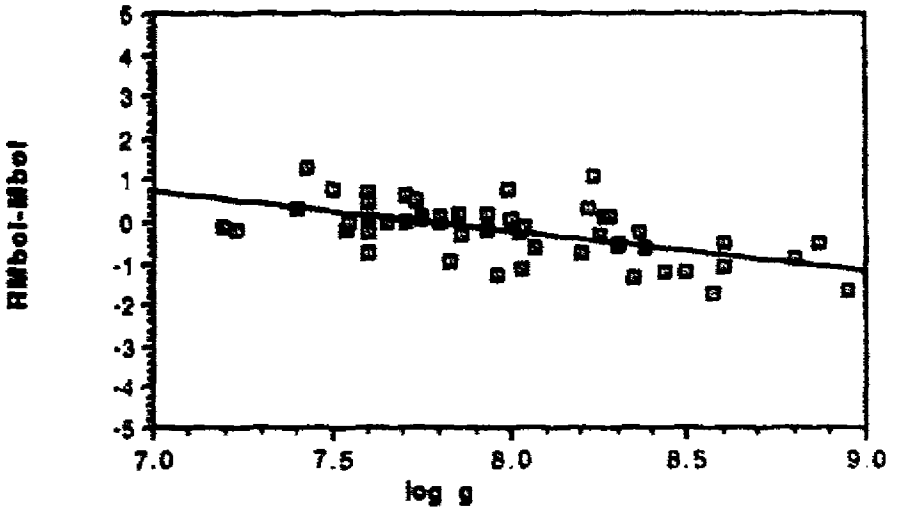

Figure 11; $^{R}M_{bol^*}-M_{bol^*}$ versus log g. This illustrates the central goal of this thesis; to demonstrate a clear relationship between bolometric magnitude and surface gravity, i.e. between brightness and mass. As predicted by theory, the slope of the line is nearly unity.

7. White Dwarfs in Clusters

A nice application of the calibration

$$^{R}M_{bol}^{*}-M_{bol}^{*} = 7.227(\pm1.504) - 0.933(\pm0.188)^{*}(\log g)$$

is to apply the magnitude corrections to white dwarfs in nearby clusters in order to determine their distance moduli as was done by van Altena (1974) for the Hyades cluster, but without log g adjustments to M_V.

The method used is as follows.

We assume that the value of $\langle\log(R_*/R_\odot)\rangle$ obtained from the main sample may be applied to stars in other clusters as well, for reasons of convenience and because it is not unreasonable that nearby white dwarfs represent a typical sample. Using this, I can calculate $^{R}M_{bol}^{*}$ for each star in a cluster. I calculate log g and T_{eff} for each star using its UBV colours, taken in this case from Agayev (1982). The Agayev catalogue is a compilation of colour, position and proper motion data for white dwarfs from numerous authors. Several values for each item are presented, where such exist. In cases of multiple data, I averaged all quoted values. ΔM_{bol}^{*} is calculated for each star using the ΔM_{bol}^{*}–log g relation obtained from Figure 11. Using the Bolometric correction–effective temperature relation from Figure 7, I then derive the absolute visual magnitude. A distance modulus follows. It is important to know, before applying this method to various clusters, how well it compares to trigonometrically–derived distances. In this vein, I derived the photometric distance moduli of such main sample stars as I had bolometric magnitudes for. The results appear in Table 12 and 13. As can be seen, the differences between photometric and trigonometric distance moduli are fairly large in many places; however, the mean difference is $\Delta(V-M_V) = 0.00$, with a scatter of ± 0.55. This large scatter would suggest that the method is as yet not extremely precise. Nevertheless, it is sufficient to give rough estimates. The results for the Hyades, after

transformation, are listed in Table 14. One star, no. 77 in Agayev, is has a distance modulus of 2.27 and is excluded as probably being a foreground star.

The mean distance modulus of these stars is 3.23, with a scatter of ± 0.10. This is nicely in accord with the distances determined by other means (see van Altena 1974). The mean distance modulus determined from the data presented by van Altena is 3.27, with a scatter of ± 0.09. The median distance modulus from van Altena is 3.25.

8. DISCUSSION

There is a definite relation between bolometric magnitude and surface gravity in DA white dwarfs, demonstrated in Figure 11. The relation of ΔM_{bol}^* to log g is not tight enough, however, to enable it to serve as a reliable method of distance estimation.

The estimated mean radius of the stars in the USNO sample is -1.91 ± 0.17, in excellent agreement with the most recently derived value of -1.90 ± 0.10 (Wiedemann 1978). The average mass of the sample is determined to be 0.50 ± 0.33 solar masses, smaller than the value determined by Bergeron et al.(1992) of 0.562 ± 0.137 solar masses. There is a rather large difference in the scatter between Bergeron et al.'s results and mine, even though our temperature and gravity results are quite similar. I think the most likely reason is that Bergeron et al. used hydrogen line profile fitting to predictions of stellar atmosphere models to determine their values, a more accurate technique than using broadband UBV data, which is more subject to contamination by outside sources. Narrow band *uvby* data would probably yield results more in accord with Bergeron et al.

The distance modulus of the Hyades cluster is found to be 3.23 ± 0.10, within the range currently accepted by photometric techniques, although closer than is suggested by geometric techniques and ZAMS-fitting.

For the future, there are several things which might be done to improve the M_{bol}^*-log g calibration and the bolometric magnitude estimates, as well as the absolute visual magnitude estimates and the distance modulus estimates. Firstly, a much larger sample of white dwarfs is desirable in order to provide a larger statistical sample with which to work. With more proper motion data and better parallaxes it would be possible to make a much more accurate estimate of the white dwarf spatial distribution, and thus calculate a more reliable absolute visual magnitude correction. Additionally, the use of intermediate band *uvby* photometry, or a narrow band system, would considerably decrease the chance of contamination by outside light sources. The use of newer model atmosphere

codes might also improve temperature and gravity estimates, and the bolometric correction. The photometry would, however, have to be done in the same survey that collected the proper motion and parallax data to ensure uniformity of the sample. This was, after all, the reason that the USNO broadband UBV data were used in this thesis in the first place.

In conclusion, this thesis has demonstrated that there is a definite relation between the luminosity, temperature and mass of white dwarfs, predicted by theory, which enables the derivation of the distance modulus of the stars in the sample. However, the scatter in derived distance moduli is rather large, and the work in this thesis should be redone using a narrow band photometric system in order to reduce errors and make the bolometric magnitude-surface gravity calibration demonstrated in this thesis more reliable.

9. Bibliography

Agayev, A.G., Guseinov, O.H., & Novruzova, H.I., 1982, Catalogue of White Dwarfs, Dordrecht Reidel

Bergeron, P., Saffer, R.A., & Liebert, J., 1992, Ap.J. 394, 228

Bevington, P.R., 1969, Data Reduction and Error Analysis for the Physical Sciences, New York , McGraw-Hill

Cox, J.P., & Guili, R.T., 1968, Principles of Stellar Structure, vol. 2, Gordon & Breach

Dahn, C.C., Harrington, R.S., Riepe, B.Y., Christy, J.W., Guetter, H.H., Kallarakal, V.V., Miranian, M., Walker, R.L., Vrba, F.J., Hewitt, A.V., Durham, W.S., & Ables, H.D., 1982, A.J. 87, 419

Dahn., C.C., Harrington, R.S., Kallarakal, V.V., Guetter, H.H., Luginbuhl, C.B., Riepe, B.Y., Walker, R.L., Pier, J.R., Vrba, F.J., Monet, D.G., & Ables, H.D., 1988 A.J. 95, 237

Eggen, O.J., & Greenstein, J.L., 1965, Ap.J. 141, 83

Greenstein, J.E., 1960, Stars and Stellar Systems, vol. 6, Chicago; University of Chicago Press

Greenham, J.A., 1972, A.J. 77, 144

Hanson, R.B., 1979, M.N.R.A.S. 186, 875

Harrington, R.S., & Dahn, C.C., 1980, A.J. 85, 454

Harrington, R.S., Dahn, C.C., Kallarakal, V.V., Riepe, B.Y., Christy, J.W., Guetter, H.H., Ables, H.D., Hewitt, A.V., Vrba, F.J., & Walker, R.L., 1985, A.J. 90, 123

Koester, D., Schulz, H., & Weidemann, V., 1979, A.A. 76, 262

Liebert, J., Dahn, C., & Monet, D., 1988, Ap.J. 332, 891

Lutz, T.E., & Kelker, D.H., 1973, P.A.S.P. 85, 573

Shipman, H.L., 1972, Ap.J. 177, 723

Shipman, H.L., Liebert, J., & Green, R.F., 1987, Ap.J. 315, 239

Sion, E.M., Greenstein, J.L., Landstreet, J.D., Liebert, J., Shipman, H.L., & Wegner, G., 1983, Ap.J. 269, 253

Trumpler, R.J., & Weaver, H.F., 1953, Statistical Astronomy, Berkely; U. of California Press

van Altena, W.F., 1974, P.A.S.P. 86, 217

Wegner, G., 1979, A.J. 84, 1384

Wegner, G., 1984, A.J. 88, 109

Wesemael, F., Auer, L.H., van Horn, H.M., & Savedoff, M.P., 1980, Ap.J.Suppl. 43, 159

Wiedemann, V., 1978, IAU Symposium no. 80 page 121, A.A.G.D.Philip &D.S. Hayes, eds

Wood, M.A., 1990, Ph.D. thesis, University of Texas at Austin

Table 1. Sorted List of log (μ) and log N(μ) Values

log (μ_{min})	log N(μ)	log (μ_{min})	log N(μ)	log (μ_{min})	log N(μ)
0.3715	0.6990	−0.3177	1.8129	−0.5418	2.0969
0.1889	1.0000	−0.3357	1.8451	−0.5627	2.1139
0.0777	1.1761	−0.3642	1.8751	−0.5832	2.1303
0.0147	1.3010	−0.3857	1.9031	−0.6024	2.1461
−0.0382	1.3979	−0.4019	1.9294	−0.6211	2.1614
−0.1007	1.4771	−0.4111	1.9542	−0.6394	2.1761
−0.1627	1.5441	−0.4183	1.9777	−0.6728	2.1903
−0.1860	1.6021	−0.4397	2.0000	−0.7016	2.2041
−0.2160	1.6532	−0.4575	2.0212	−0.8204	2.2175
−0.2566	1.6990	−0.4773	2.0414	−0.9126	2.2304
−0.2715	1.7404	−0.4928	2.0607	−1.1057	2.2405
−0.2822	1.7782	−0.5222	2.0792		

Table 2. White Dwarf Positions, Proper Motions and Parallaxes (USNO lists)

Star	Location(Epoch 2000) h / m / s	deg/min	μ (" / yr)	±	π_o (")	±
LP49-275	00 05 07	73 13.2	0.2284	0.0026	0.0288	0.0032
G217-37	00 12 14	50 25.2	0.7189	0.0015	0.0907	0.0025
W1	00 13 39	00 19.3	0.4646	0.0016	0.0337	0.0048
L795-44	00 33 54	-12 08.0	0.2399	0.0011	0.0039	0.0055
L1011-71	00 35 35	01 53.1	0.3840	0.0011	0.0285	0.0048
L1011-92	00 41 22	55 50.1	0.3253	0.0018	0.0473	0.0029
W28	00 49 10	05 23.4	2.9608	0.0017	0.2322	0.0027
G1-45	01 03 50	05 04.6	0.3996	0.0010	0.0478	0.0038
W1516	01 17 59	16 10.2	0.6432	0.0018	0.0623	0.0034
G133-8	01 24 21	40 23.8	0.7016	0.0016	0.0324	0.0055
W72	01 29 23	10 23.1	0.4015	0.0019	0.0291	0.0031
R548	01 36 11	-11 20.8	0.2400	0.0005	0.0158	0.0020
L870-2	01 37 59	-04 59.8	0.6875	0.0032	0.0831	0.0032
G72-31	01 45 11	31 32.8	0.3457	0.0010	0.0287	0.0043
LP768-500	01 48 08	-17 12.3	1.1044	0.0018	0.0125	0.0100
OXF+25 6	02 08 47	25 14.2	0.4302	0.0016	0.0315	0.0029
G74-7	02 11 21	39 55.2	1.1344	0.0019	0.0651	0.0040
G134-22	02 16 59	42 57.9	1.0344	0.0016	0.0525	0.0044
LP710-47	02 32 38	-14 11.9	0.6801	0.0015	0.0648	0.0040
Feige 24	02 35 06	03 44.1	0.0784	0.0019	0.0135	0.0029
G75-39	02 46 30	-02 27.6	0.5317	0.0013	0.0478	0.0050
G174-14	02 47 38	54 23.3	0.5724	0.0002	0.0966	0.0031
G76-48	02 59 59	08 11.8	0.4812	0.0008	0.0364	0.0035
W219	03 34 34	18 26.5	1.1959	0.0010	0.0541	0.0038
G37-44	03 35 17	32 11.9	0.3766	0.0020	0.0116	0.0044
G7-16	04 00 26	08 14.1	0.5368	0.0018	0.0565	0.0037
LB1240	04 04 34	25 08.9	0.2294	0.0016	0.0373	0.0028
G38-29	04 20 18	36 16.4	0.2783	0.0017	0.0135	0.0041
STN2051B	04 31 14	58 58.1	2.3525	0.0008	0.1819	0.0034
G39-27	04 36 45	27 09.8	0.2737	0.0007	0.0601	0.0033
L879-14	04 37 48	-08 49.2	1.5616	0.0006	0.1055	0.0027
G175-46	04 43 59	51 06.4	0.4779	0.0013	0.0214	0.0035
GD64	04 57 21	41 56.0	0.2101	0.0021	0.0228	0.0026
G191-B2B	05 05 30	52 48.8	0.0884	0.0017	0.0219	0.0026
LP777-1	05 05 53	-17 22.8	0.6827	0.0019	0.0460	0.0040
G86-B1B	05 21 43	33 22.0	0.2124	0.0009	0.0092	0.0034
LP119-48	05 29 50	52 39.9	0.6516	0.0020	0.0239	0.0034
G98-18	05 37 12	32 15.0	0.4114	0.0015	0.0039	0.0042
G99-37	05 51 20	00 12.1	0.2695	0.0015	0.0902	0.0028
G102-39	06 53 53	12 24.1	0.2558	0.0018	0.0151	0.0053

Table 2. Continued

Star	Location h / m / s	deg/min	μ (" / yr)	±	π_0 (")	±
HL4	05 55 10	-04 10.7	2.3782	0.0032	0.1557	0.0050
G99-47	05 56 25	05 21.6	1.0213	0.0009	0.1249	0.0036
L1244-26	06 15 18	17 43.5	0.3534	0.0014	0.0238	0.0031
G105-30	06 20 48	06 45.3	0.5350	0.0012	0.0440	0.0042
G108-26	06 47 22	02 31.1	0.4094	0.0013	0.0542	0.0037
HE3	06 47 38	37 30.8	0.9561	0.0018	0.0693	0.0025
LP58-53	06 53 24	64 03.8	0.4192	0.0011	0.0303	0.0052
G108-42	06 57 23	02 40.9	0.2098	0.0006	0.0260	0.0037
G87-29	07 10 14	37 40.3	0.3493	0.0029	0.0444	0.0036
G107-70	07 30 47	48 10.0	1.2837	0.0005	0.0904	0.0028
L745-46A	07 40 20	-17 24.9	1.2679	0.0017	0.1108	0.0032
G90-28	07 55 25	36 21.8	0.3898	0.0015	0.0298	0.0043
G193-78	07 56 01	57 41.9	0.4370	0.0017	0.0288	0.0038
G111-54	08 05 32	38 32.2	0.2883	0.0014	0.0245	0.0030
G111-71	08 20 00	38 34.5	0.3083	0.0009	0.0199	0.0041
G51-16	08 30 39	32 41.8	0.5352	0.0008	0.0454	0.0038
G47-18	08 59 14	32 57.0	0.3235	0.0009	0.0494	0.0034
G195-19	09 15 54	53 25.2	1.5450	0.0008	0.0979	0.0024
G116-16	09 16 42	43 59.7	0.2489	0.0013	0.0352	0.0041
G117-B15A	09 24 16	35 16.9	0.1368	0.0019	0.0143	0.0053
G161-36	09 29 22	-04 10.3	0.2262	0.0008	0.0224	0.0032
G117-25	09 33 41	29 11.3	0.2326	0.0018	0.0318	0.0046
SA29-130	09 46 39	43 55.2	0.3005	0.0018	0.0301	0.0030
G195-42	09 50 16	53 15.1	0.2630	0.0021	0.0442	0.0036
G49-33	09 57 48	24 32.8	0.3997	0.0014	0.0415	0.0045
G260-15	10 00 11	70 40.0	0.5218	0.0023	0.0783	0.0035
G43-38	10 15 03	08 06.5	0.3241	0.0010	0.0351	0.0040
G53-38	10 16 07	-01 19.3	0.5090	0.0012	0.0239	0.0043
G235-67	10 23 10	63 27.7	0.3838	0.0021	0.0619	0.0037
G44-32	10 41 54	14 15.7	0.3052	0.0011	0.0228	0.0035
LP93-21	10 45 58	59 04.0	1.7764	0.0009	0.0014	0.0054
L898-25	10 57 40	-07 31.0	0.7931	0.0009	0.0856	0.0042
LB253	11 07 42	59 58.4	0.2393	0.0014	0.0235	0.0044
L971-14	11 18 15	-03 14.1	0.5845	0.0010	0.0271	0.0051
R627	11 24 12	12 21.6	1.0269	0.0017	0.0734	0.0032
G122-31	11 34 47	46 48.5	0.1988	0.0015	0.0148	0.0051
G148-7	11 45 57	31 49.9	0.2872	0.0014	0.0331	0.0033
L1405-40	11 50 20	25 18.5	0.3059	0.0014	0.0211	0.0038
L1261-24	11 56 44	18 22.3	0.3332	0.0012	0.0327	0.0041
G197-47	12 11 28	57 24.3	0.5532	0.0007	0.0495	0.0047

Table 2. Continued

Star	Location h / m / s	deg/min	μ (″/yr)	±	π_0 (″)	±
C1	12 15 45	52 31.2	0.1205	0.0014	0.0334	0.0041
G148-B4B	12 17 34	32 05.3	0.2573	0.0012	0.0267	0.0062
G61-17	12 47 15	14 41.9	0.3846	0.0006	0.0166	0.0043
L1408-19	12 59 46	27 34.0	0.3310	0.0010	0.0298	0.0043
W457	13 00 09	03 28.7	0.9600	0.0006	0.0605	0.0042
HZ43	13 16 21	29 06.1	0.1718	0.0016	0.0155	0.0034
G199-71	13 27 40	57 55.1	0.4323	0.0013	0.0277	0.0055
W485A	13 30 13	-08 34.6	1.1775	0.0017	0.0647	0.0032
G165-7	13 31 00	30 29.8	0.4707	0.0012	0.0343	0.0054
GD325	13 36 01	48 28.7	0.1223	0.0022	0.0295	0.0035
W489	13 36 29	03 40.5	3.8958	0.0021	0.1197	0.0042
G63-54	13 47 24	10 21.5	0.8957	0.0013	0.0508	0.0036
LP380-5	13 48 03	23 34.8	1.4690	0.0024	0.0796	0.0032
L1484-18	14 10 27	32 08.4	0.2389	0.0019	0.0265	0.0028
G124-26	14 20 53	-09 05.2	0.4565	0.0010	0.0255	0.0039
G200-39	14 27 35	53 48.0	0.3695	0.0018	0.0183	0.0039
GD337	14 34 42	53 35.5	0.1259	0.0044	0.0046	0.0054
L1126-68	14 50 49	07 33.5	0.9157	0.0019	0.0056	0.0045
G166-58	14 58 06	29 37.3	0.6082	0.0017	0.0298	0.0041
GD175	15 05 51	-07 14.7	0.1971	0.0015	0.0393	0.0055
GD178	15 11 27	32 04.3	0.1539	0.0032	0.0219	0.0042
LP68-60	15 19 48	63 29.8	0.2483	0.0046	0.0168	0.0070
R808	16 01 23	36 48.4	0.5539	0.0018	0.0370	0.0046
G138-8	16 11 25	13 22.2	0.5364	0.0014	0.0577	0.0047
LP444-31	16 13 02	16 31.9	0.2105	0.0023	0.0161	0.0044
G138-31	16 27 53	09 12.2	0.4745	0.0026	0.0468	0.0060
R640	16 28 24	36 46.5	0.8979	0.0013	0.0611	0.0049
LP101-16	16 34 18	57 10.0	1.6315	0.0027	0.0627	0.0061
G180-63	16 35 01	43 17.4	0.3771	0.0018	0.0670	0.0031
G138-47	16 37 40	13 40.6	0.2367	0.0015	0.0261	0.0046
L1491-27	16 39 28	33 25.1	0.4616	0.0009	0.0342	0.0038
G138-56	16 41 36	15 12.4	0.6641	0.0040	0.0073	0.0100
GD358	16 47 18	32 28.4	0.1512	0.0025	0.0280	0.0034
G226-29	16 48 26	59 03.3	0.3358	0.0037	0.0827	0.0046
G169-34	16 57 09	21 26.6	0.5600	0.0012	0.0435	0.0031
G139-13	17 08 07	02 57.4	0.3964	0.0011	0.0574	0.0054
A+69 6829	17 13 05	69 31.2	0.3633	0.0031	0.0400	0.0044
W672A	17 18 35	01 56.9	0.5222	0.0024	0.0245	0.0042
G140-2	17 38 41	05 16.0	0.2860	0.0014	0.0237	0.0039
LP44-113	17 48 03	70 52.9	1.6725	0.0024	0.1657	0.0037

Table 2. Continued

Star	Location h / m / s	deg/min	μ (″ / yr)	±	z_0 (°)	±
LP9-231	17 56 47	82 43.9	3.5888	0.0034	0.0592	0.0048
G206-18	18 13 31	32 48.5	0.2498	0.0034	0.0199	0.0076
G206-17	18 13 31	32 48.5	0.2506	0.0025	0.0199	0.0053
L1208132	18 20 32	12 38.9	0.2611	0.0024	0.0246	0.0055
LP103-294	18 21 19	61 00.8	0.7155	0.0026	0.0786	0.0041
R137	18 27 13	04 0.37	0.3752	0.0019	0.0150	0.0032
L993-18	18 29 09	-04 29.8	0.2924	0.0013	0.0354	0.0038
G227-35	18 30 19	54 47.6	0.3817	0.0033	0.0673	0.0039
G184-12	18 33 59	19 45.8	0.3952	0.0019	0.0187	0.0048
GD215	18 43 25	04 20.4	0.1421	0.0024	0.0403	0.0034
L922-82	18 49 48	-09 57.9	0.2020	0.0031	0.0358	0.0040
L1498-12	18 57 50	33 57.5	0.3544	0.0023	0.0308	0.0044
G125-3	19 18 58	38 43.4	0.2498	0.0019	0.0857	0.0034
L923-21	19 20 36	-07 39.5	0.1830	0.0026	0.1006	0.0042
G185-32	19 37 14	27 43.3	0.4422	0.0018	0.0560	0.0029
GD222	19 38 28	32 53.3	0.1419	0.0200	0.0291	0.0025
L1573-31	19 42 17	37 32.3	0.2140	0.0023	0.0208	0.0028
L1285-97	19 45 32	16 27.5	0.2928	0.0016	0.0241	0.0027
L997-21	19 56 29	-01 02.7	0.8227	0.0019	0.0840	0.0037
LP754-16	20 05 34	-10 56.7	1.0684	0.0020	0.0571	0.0055
GD229	20 12 22	31 13.7	0.1012	0.0018	0.0348	0.0027
G24-9	20 13 55	06 42.7	0.6319	0.0018	0.0398	0.0050
W1346	20 34 20	25 03.7	0.6957	0.0024	0.0689	0.0035
G187-8	20 50 20	26 30.5	0.5097	0.0017	0.0499	0.0034
VB11	20 56 45	-04 50.6	0.8084	0.0015	0.0628	0.0055
L1504-14	21 01 44	31 48.6	0.3933	0.0023	0.0296	0.0035
G144-51	21 02 03	19 12.8	0.3215	0.0025	0.0263	0.0044
G187-16	21 02 12	24 57.8	0.3881	0.0019	0.0363	0.0042
G25-20	21 13 27	07 26.4	0.3487	0.0016	0.0416	0.0038
L1433-34	21 13 46	26 21.4	0.3931	0.0020	0.0317	0.0037
R198	21 26 25	55 13.6	0.3388	0.0030	0.0301	0.0044
G261-43	21 26 57	73 18.6	0.3149	0.0027	0.0433	0.0035
L1002-16	21 32 16	00 15.1	0.4259	0.0017	0.0253	0.0031
G261-45	21 33 44	83 03.7	0.6282	0.0014	0.0322	0.0058
G212-45	21 35 18	46 33.2	0.4316	0.0017	0.0300	0.0061
G126-18	21 38 46	23 09.4	0.2974	0.0012	0.0240	0.0031
G126-25	21 42 08	13 28.6	0.3453	0.0039	0.0058	0.0125
L1363-3	21 42 40	20 59.8	0.6711	0.0023	0.0748	0.0037
L930-80	21 47 37	-07 44.2	0.2847	0.0021	0.0146	0.0021
G188-27	21 49 53	28 17.2	0.2658	0.0021	0.0287	0.0030

Table 2. Continued

Star	Location h / m / s	deg/min	μ ("/yr)	±	π_0 (")	±
G93-48	22 52 25	02 23.3	0.2712	0.0017	0.0409	0.0025
G18-34	22 09 47	14 29.9	0.3612	0.0009	0.0398	0.0044
G241-6	22 23 35	68 37.2	0.2836	0.0015	0.0147	0.0044
G28-13	22 43 04	-01 27.8	0.2327	0.0011	0.0096	0.0057
G67-23	22 49 06	22 36.4	0.5254	0.0015	0.0529	0.0041
G128-7	22 51 24	29 39.8	1.2588	0.0016	0.0495	0.0047
G156-64	22 55 50	-07 50.0	0.5527	0.0011	0.0251	0.0069
L935-50	23 14 27	-06 33.1	0.3881	0.0020	0.0403	0.0048
G157-35	23 15 19	-02 09.8	0.6156	0.0016	0.0392	0.0059
G29-38	23 28 47	05 14.8	0.5258	0.0024	0.0736	0.0042
L1440-18	23 32 04	26 58.7	0.4330	0.0014	0.0264	0.0047
L1512-34	23 43 54	32 32.8	0.2221	0.0009	0.0598	0.0031
G130-15	23 49 54	29 33.9	0.4976	0.0020	0.0470	0.0041
G171-27	23 54 57	40 27.4	0.5698	0.0020	0.0389	0.0038

Table 3. Magnitudes and Colours

Star	V	±	B–V	±	U–B	±	Type*
LP49-275	14.33	0.01	–0.07	0.01	–0.91	0.01	-
G217-37	14.36	0.00	0.42	0.01	–0.42	0.03	-
W1	15.34	0.00	0.21	0.02	–0.54	0.03	-
L795-44	14.88	0.01	0.67	0.01	–0.06	0.02	-
L1011-71	15.61	0.03	0.20	0.03	–0.66	0.05	-
L1011-92	14.06	0.00	0.05	0.01	–0.81	0.01	-
W28	12.39	0.00	0.54	0.00	0.02	0.01	-
G1-45	13.96	0.01	0.31	0.01	–0.57	0.03	DA
W1516	13.83	0.02	0.14	0.02	–0.77	0.03	DC
G133-8	17.10	0.02	0.82	0.06	0.21	0.05	-
W72	14.38	0.01	0.26	0.01	–0.54	0.02	-
R548	14.16	0.02	0.17	0.01	–0.50	0.01	-
L870-2	12.86	0.01	0.34	0.00	–0.48	0.02	DAs
G72-31	14.80	0.02	0.20	0.01	–0.56	0.02	-
LP768-500	17.66		0.43		–0.50		-
OXF+25 6	13.23	0.02	–0.04	0.01	–0.84	0.02	DA?
G74-7	14.51	0.01	0.37	0.07	–0.43	0.06	-
G134-22	16.19	0.01	0.72	0.02	–0.02	0.04	-
LP710-47	15.76	0.01	0.75	0.02	–0.01	0.03	-
Feige 24	12.42	0.01	–0.20	0.01	–1.16	0.01	-
G75-39	15.53	0.02	0.36	0.02	–0.51	0.03	-
G174-14	15.32	0.01	0.93	0.01	0.35	0.02	-
G76-48	15.90	0.02	0.43	0.01	–0.41	0.01	-
W219	15.18	0.02	0.31	0.01	–0.55	0.01	C_2
G37-44	15.49	0.04	0.13	0.04	–0.51	0.03	-
G7-16	15.87	0.02	0.70	0.01	0.00	0.02	-
LB1240	13.81	0.02	0.12	0.01	–0.58	0.01	DA
G38-29	15.59	0.06	0.24	0.04	–0.55	0.05	-
STN2051B	12.44		0.31		–0.53		DC
G39-27	15.79	0.01	0.65	0.01	–0.04	0.02	DC
L879-14	13.76	0.00	0.32	0.01	–0.53	0.01	C_2
G175-46	15.96	0.04	0.21	0.04	–0.61	0.01	..
GD64	14.00	0.01	0.07	0.01	–0.63	0.01	DA
G191-B2B	11.78	0.03	–0.34	0.02	–1.20	0.00	-
LP777-1	15.97	0.01	0.74	0.01	0.00	0.01	-
G86-B1B	16.09	0.02	0.26	0.01	–0.61	0.01	-
LP119-48	15.56	0.00	0.00	0.01	–0.97	0.01	-
G98-18	16.43	0.06	0.38	0.01	–0.59	0.08	-
G99-37	14.53	0.01	0.50	0.01	–0.46	0.01	C_{2p}
G102-39	15.92	0.02	–0.12	0.01	–0.74	0.01	-

Table 3. Continued

Star	V	±	B–V	±	U–B	±	Type*
HL4	14.45	0.01	1.04	0.01	0.76	0.05	-
G99–47	14.10	0.02	0.59	0.01	–0.17	0.02	-
L1244–26	13.39	0.01	–0.17	0.01	–0.97	0.01	
G105–30	16.37	0.00	0.55	0.00	–0.17	0.00	-
G108–26	15.68	0.01	0.32	0.01	–0.53	0.01	-
HE3	12.05	0.02	–0.09	0.00	0.92	0.01	DAn
LP58–53	16.64	0.02	0.52	0.03	–0.17	0.02	-
G108–42	16.22	0.10	0.09	0.01	–0.72	0.02	-
G87–29	15.54	0.03	0.33	0.04	–0.53	0.04	4o70
G107–70	14.64	0.01	0.99	0.02	0.34	0.03	DC
L745–46A	13.04	0.00	0.24	0.00	–0.62	0.00	
G90–28	16.07	0.00	0.26	0.01	–0.43	0.06	
G193–78	15.08	0.01	0.08	0.01	–0.79	0.00	DC
G111–54	15.56	0.00	0.06	0.03	–0.86	0.05	DFp
G111–71	16.55	0.02	0.26	0.01	–0.56	0.02	-
G51–16	15.73	0.01	0.29	0.01	–0.54	0.03	-
G47–18	15.18	0.05	0.01	0.04	–0.93	0.00	4o70, C2p
G195–19	13.85	0.00	0.34	0.01	–0.52	0.02	DC, DXp
G116–16	15.37	0.00	0.21	0.01	–0.57	0.04	DAs
G117B15A	15.50	0.01	0.17	0.01	–0.62	0.02	DA
G161–36	14.76	0.02	0.12	0.01	–0.59	0.02	-
G117–25	15.91	0.04	0.23	0.04	–0.59	0.04	-
SA29–130	13.30	0.01	0.07	0.01	–0.57	0.01	DA
G195–42	15.20	0.01	0.13	0.02	–0.70	0.02	DC, C2
G49–33	15.07	0.03	0.24	0.01	–0.63	0.01	DA
G260–15	13.20	0.02	0.04	0.01	–0.86	0.01	-
G43–38	16.04	0.02	0.40	0.02	–0.46	0.02	
G53–38	15.37	0.01	0.26	0.01	–0.50	0.02	
G235–67	14.71	0.00	0.36	0.00	–0.49	0.02	-
G44–32	16.52	0.02	0.31	0.01	–0.58	0.01	
LP93–21	17.94		0.13		–0.85		-
L898–25	14.33	0.02	0.32	0.02	–0.53	0.01	DA
LB253	13.79	0.01	–0.02	0.02	–0.78	0.02	-
L971–14	15.40	0.05	0.05	0.04	–0.74	0.03	-
R627	14.32	0.07	0.26	0.02	–0.50	0.03	DF, DAF
G122–31	16.39	0.03	0.01	0.03	–0.93	0.04	-
G148–7	13.65	0.04	0.05	0.02	–0.68	0.01	DAn, DAn
L1405–40	15.67	0.01	0.20	0.03	–0.60	0.03	-
L1261–24	15.63	0.01	0.23	0.01	–0.58	0.03	DC
G197–47	15.79	0.01	0.58	0.01	–0.20	0.02	-

Table 3. Continued

Star	V	±	B–V	±	U–B	±	Type*
C1	13.30	0.01	0.50	0.00	–0.49	0.01	DA
G148–B4B	17.00		0.35		–0.49		–
G61–17	15.86	0.02	0.20	0.01	–0.55	0.01	–
L1408–19	15.39	0.01	0.25	0.03	–0.61	0.02	DAs
W457	15.77	0.02	0.64	0.02	–0.11	0.05	–
HZ43	12.68	0.01	–0.12	0.01	–1.17	0.01	–
G199–71	16.70	0.03	0.42	0.03	–0.43	0.04	–
W485A	12.31	0.01	0.09	0.01	–0.62	0.01	DA, DA
G165–7	16.04	0.01	0.72	0.02	0.78	0.03	–
GD325	14.00	0.02	0.01	0.01	–0.94	0.01	–
W489	14.63	0.05	0.96	0.09	0.29	0.05	DK
G63–54	15.08	0.05	0.41	0.02	–0.49	0.05	DAwk
LP380–5	15.64	0.00	1.10	0.01	0.47	0.02	–
L1484–18	13.97	0.01	–0.01	0.02	–0.76	0.01	–
G124–26	15.36	0.02	0.33	0.02	–0.58	0.00	–
G200–39	15.04	0.02	–0.07	0.01	–0.98	0.01	–
GD337	16.09	0.01	–0.03	0.01	–0.88	0.02	–
L1126–68	15.46	0.04	0.04	0.05	–0.67	0.01	–
G166–58	15.59	0.04	0.27	0.04	–0.50	0.02	–
GD175	15.89	0.01	0.38	0.03	–0.62	0.01	DA
GD 178	14.12	0.01	0.06	0.03	–0.62	0.01	DA
LP68–60	16.63	0.02	–0.04	0.02	–0.94	0.06	–
R808	14.36		0.17		–0.56	0.00	DA
G138–8	15.09	0.01	0.23	0.02	–0.64	0.05	–
LP444–31	15.67	0.02	0.07	0.03	–0.63	0.02	–
G138–31	16.12	0.01	0.37	0.20	–0.44	0.01	–
R640	13.85	0.01	0.16	0.02	–0.66	0.01	DFp, DFp
LP101–16	15.00		0.49		–0.36	0.00	–
G180–63	14.82	0.02	0.41	0.02	–0.41	0.02	–
G138–47	16.90		0.41		–0.50		–
L1491–27	14.66	0.01	0.18	0.01	–0.57	0.01	–
G138–56	15.70	0.09	0.41	0.10	–0.63		–
GD358	13.65		–0.11		–1.04		DB
G226–29	12.24	0.01	0.16	0.00	–0.62	0.01	–
G169–34	14.04	0.01	0.26	0.04	–0.52	0.01	DAss, DAss
G139–13	15.17	0.04	0.48	0.03	–0.21	0.09	–
A+696829	13.26		0.05		–0.69		–
W672A	14.36	0.00	0.11	0.01	–0.58	0.01	DA?
G140–2	15.86	0.02	0.46	0.03	–0.80	0.07	–
LP44–113	14.15	0.01	0.40	0.01	–0.30	0.02	–

Table 3. Continued

Star	V	±	B–V	±	U–B	±	Type*
LP9–231	14.29	0.00	0.37	0.01	–0.52	0.02	DAss
G206–18	17.24	0.21	0.50	0.06			–
G206–17	16.40	0.02	0.28	0.02			–
L1208132	15.86	0.06	0.55	0.03	–0.17	0.04	–
LP103–294	15.65	0.02	0.97	0.03	0.98	0.04	–
R137	13.93	0.06	0.04	0.06	–0.45	0.10	–
L993–18	14.57	0.01	0.24	0.03	–0.60	0.01	–
G227–35	15.50	0.02	0.49	0.02	–0.44	0.00	–
G184–12	16.45	0.02	0.26	0.04	–0.58	0.05	–
GD215	14.92	0.03	0.14	0.02	–0.59	0.02	DAss, DAss
L922–82	14.20	0.00	0.23	0.00			–
L1498–12	14.62	0.02	0.16	0.02	–0.61	0.01	–
G125–3	14.58	0.04	0.44	0.05	–0.36	0.03	–
L923–21	12.28	0.02	0.07	0.01	–0.81	0.01	–
G185–32	12.97	0.01	0.17	0.01	–0.56	0.00	DA
GD222	13.59		–0.08		–0.90		DA
L1573–31	14.52	0.01	–0.08	0.01	–0.98	0.02	DB, DB
L1285–97	13.99	0.00	–0.03	0.01	–0.81	0.01	–
L997–21	13.71	0.05	0.30	0.00	–0.61	0.05	DAs
LP754–16	16.87	0.05	1.04	0.07			–
GD229	14.85	0.02	–0.08	0.01	–1.22	0.03	DXp
G24–9	15.73	0.02	0.36	0.01	–0.39	0.03	–
W1346	11.51	0.00	–0.07	0.01	–0.87	0.01	DA
G187–8	15.58	0.03	0.95	0.02	0.40	0.02	–
VB11	16.56	0.03	1.18	0.03			–
L1504–14	15.07	0.02	0.10	0.03	–0.79	0.02	–
G144–51	16.40	0.05	0.37	0.07	–0.39	0.04	–
G187–16	16.57	0.01	0.50	0.02	–0.28	0.03	–
G25–20	16.17	0.02	0.45	0.02	–0.36	0.02	–
L1433–34	14.69	0.01	0.25	0.02	–0.54	0.01	–
R198	14.75	0.00	0.13	0.00	–0.69	0.00	–
G261–43	12.78	0.02	0.02	0.04	–0.65	0.00	DA
L1002–16	14.763	0.01	–0.15	0.02	–0.92	0.02	–
G261–45	13.02	0.00	0.00	0.01	–0.72	0.00	DA
G212–45	16.05	0.12	0.70	0.18	0.34	0.11	–
G126–18	15.25	0.04	0.14	0.01	–0.50	0.02	DA
G126–25	16.58	0.02	0.29	0.02	–0.56	0.01	–
L1363–3	13.24	0.02	0.16	0.01	–0.70	0.01	DC
L930–80	14.83	0.03	–0.11	0.04	–0.94	0.03	–
G188–27	14.68	0.02	–0.01	0.02	–0.88	0.02	DC

Table 3. Continued

Star	V	±	B–V	±	U–B	±	Type*
G93–48	12.73	0.03	0.06	0.04	–0.77	0.01	DA
G18–34	15.66	0.03	0.23	0.02	–0.54	0.03	–
G241–6	15.65	0.01	–0.05	0.01	–0.95		–
G28–13	16.14	0.04	0.27	0.07	–0.51	0.09	–
G67–23	14.37	0.01	0.17	0.01	–0.67	0.01	DA
G128–7	15.52	0.01	0.61	0.01	–0.10	0.07	–
G156–64	16.47	0.01	0.45	0.04	–0.47	0.01	–
L935–50	15.42	0.01	0.22	0.01	–0.63	0.01	–
G157–35	16.29	0.02	0.51	0.03	–0.37	0.03	–
G29–38	13.03	0.02	0.14	0.01	–0.63	0.02	DA
L1440–18	15.33	0.02	0.19	0.03	–0.63	0.03	–
L1512–34	12.93	0.01	0.14	0.02	–0.61	0.02	–
G130–15	15.72	0.01	0.58	0.01	–0.24	0.02	–
G171–27	14.94	0.01	0.18	0.01	–0.68	0.02	C_2

* Note: See Graham (1972) and Wegner (1984); Graham uses older system

Table 4. Adjusted Absolute Magnitudes for White Dwarf Sample

Star	Epsilon	Mv (uncorr)	±	Correction	Mv (Corr)	±
LP49–275	0.1111	11.63	0.24	–0.06	11.57	0.24
G217–37	0.0276	14.15	0.06	–0.01	14.14	0.06
W1	0.1424	12.98	0.31	–0.15	12.83	0.32
L795–44	1.4103	7.85	3.04	–2.85	5.00	91.79
L1011–71	0.1684	12.88	0.37	–0.21	12.67	0.39
L1011–92	0.0613	12.43	0.14	–0.02	12.41	0.14
W28	0.0116	14.22	0.03	0.00	14.22	0.03
G1–45	0.0795	12.36	0.18	–0.04	12.32	0.18
W1516	0.0546	12.80	0.12	–0.02	12.78	0.12
G133–8	0.1698	14.65	0.37	–0.22	14.43	0.39
W72	0.1287	11.70	0.25	–0.08	11.62	0.25
R548	0.2371	10.15	0.32	–0.09	10.06	0.32
L870–2	0.0451	12.46	0.09	–0.01	12.45	0.09
G72–31	0.1305	12.09	0.33	–0.12	11.97	0.34
LP768–500	0.2997	13.15	1.74	–2.00	11.15	17.70
OXF+25 6	0.1189	10.72	0.23	–0.06	10.66	0.23
G74–7	0.0575	13.58	0.13	–0.03	13.55	0.13
G134–22	0.0714	14.79	0.18	–0.05	14.74	0.18
LP710–47	0.0578	14.82	0.13	–0.03	14.79	0.13
Feige 24	0.2775	8.08	0.47	–0.18	7.90	0.48
G75–39	0.0784	13.93	0.23	–0.08	13.85	0.23
G174–14	0.0388	15.24	0.07	–0.01	15.23	0.07
G76–48	0.1029	13.70	0.21	–0.07	13.63	0.21
W219	0.0692	13.84	0.16	–0.03	13.81	0.16
G37–44	0.3229	10.82	0.83	–1.04	9.78	1.51
G7–16	0.0663	14.63	0.15	–0.03	14.60	0.15
LB1240	0.1004	11.67	0.17	–0.03	11.64	0.17
G38–29	0.2775	11.25	0.66	–0.57	10.68	0.78
STN2051B	0.0206	13.74	0.04	0.00	13.74	0.04
G39–27	0.0623	14.68	0.12	–0.02	14.66	0.12
L879–14	0.0355	13.88	0.06	–0.00	13.88	0.06
G175–46	0.1751	12.61	0.36	–0.20	12.41	0.38
GD64	0.1643	10.79	0.25	–0.05	10.74	0.25
G191–B2B	0.1711	8.48	0.26	–0.05	8.43	0.26
LP777–1	0.0814	14.29	0.19	–0.05	14.24	0.19
G86–B1B	0.4072	10.90	0.81	–0.62	10.28	0.93
LP119–48	0.1567	12.45	0.31	–0.15	12.30	0.32
G98–18	0.9606	9.39	2.34	–2.15	7.24	54.71
G99–37	0.0415	14.31	0.07	–0.00	14.31	0.07
G102–39	0.2481	11.82	0.76	–0.77	11.05	0.99

Table 4. Continued

Star	Epsilon	Mv (uncorr)	±	Correction	Mv (Corr)	±
HL4	0.0241	15.41	0.07	–0.01	15.40	0.07
G99–47	0.0300	14.58	0.07	–0.01	14.57	0.07
L1244–26	0.1574	10.27	0.29	–0.12	10.15	0.30
G105–30	0.0851	14.59	0.21	–0.06	14.53	0.21
G108–26	0.0691	14.35	0.15	–0.03	14.32	0.15
HE3	0.0541	11.25	0.08	–0.01	11.24	0.08
LP58–53	0.1236	14.05	0.37	–0.22	13.83	0.39
G108–42	0.1441	13.29	0.31	–0.07	13.22	0.31
G87–29	0.0844	13.78	0.18	–0.03	13.75	0.18
G107–70	0.0414	14.42	0.07	–0.01	14.41	0.07
L745–46A	0.0338	13.26	0.06	–0.01	13.25	0.06
G90–28	0.1257	13.44	0.32	–0.15	13.29	0.33
G193–78	0.1301	12.38	0.29	–0.13	12.25	0.30
G111–54	0.1529	12.50	0.27	–0.08	12.42	0.27
G111–71	0.1882	13.05	0.45	–0.24	12.81	0.47
G51–16	0.0825	14.01	0.19	–0.05	13.96	0.19
G47–18	0.0758	13.65	0.16	–0.02	13.63	0.16
G195–19	0.0383	13.80	0.06	–0.00	13.80	0.06
G116–16	0.1064	13.10	0.25	–0.07	13.03	0.25
G117–B15A	0.2620	11.28	0.81	–0.63	10.65	0.93
G161–36	0.1672	11.51	0.31	–0.11	11.40	0.32
G117–25	0.1178	13.42	0.32	–0.11	13.31	0.33
SA29–130	0.1245	10.69	0.23	–0.05	10.64	0.23
G195–42	0.0848	13.43	0.18	–0.03	13.40	0.18
G49–33	0.0903	13.16	0.24	–0.08	13.08	0.24
G260–15	0.0478	12.67	0.10	–0.01	12.66	0.10
G43–38	0.1067	13.77	0.25	–0.07	13.70	0.25
G53–38	0.1567	12.26	0.40	–0.25	12.01	0.43
G235–67	0.0605	13.67	0.13	–0.02	13.65	0.13
G44–32	0.1643	13.31	0.34	–0.13	13.18	0.35
LP93–21	0.3286	13.23	1.03	–1.40	11.83	2.85
L898–25	0.0438	13.99	0.11	–0.02	13.97	0.11
LB253	0.1594	10.65	0.42	–0.20	10.45	0.44
L971–14	0.1382	12.57	0.42	–0.27	12.30	0.45
R627	0.0510	13.65	0.12	–0.01	13.64	0.12
G122–31	0.2531	12.24	0.76	–0.53	11.71	0.84
G148–7	0.1132	11.25	0.24	–0.05	11.20	0.24
L1405–40	0.1775	12.29	0.40	–0.18	12.11	0.41
L1261–24	0.1146	13.20	0.27	–0.08	13.12	0.27
G197–47	0.0757	14.26	0.21	–0.06	14.20	0.21

Table 4. Continued

Star	Epsilon	My (uncorr)	±	Correction	My (Corr)	±
C1	0.1122	10.92	0.27	-0.05	10.87	0.27
G148-B4B	0.1403	14.13	0.00	-0.32	13.81	0.20
G61-17	0.2257	11.96	0.56	-0.53	11.43	0.69
L1408-19	0.1257	12.76	0.31	-0.11	12.65	0.32
W457	0.0619	14.68	0.15	-0.03	14.65	0.15
HZ43	0.2417	8.63	0.48	-0.19	8.44	0.49
G199-71	0.1352	13.91	0.44	-0.30	13.61	0.48
W485A	0.0579	11.36	0.12	-0.02	11.34	0.12
G165-7	0.1092	13.72	0.34	-0.18	13.54	0.36
GD325	0.1270	11.35	0.26	-0.05	11.30	0.26
W489	0.0313	15.02	0.09	-0.01	15.01	0.09
G63-54	0.0737	13.61	0.17	-0.03	13.58	0.17
LP380-5	0.0471	15.14	0.09	-0.11	15.03	0.09
L1484-18	0.1414	11.08	0.25	-0.06	11.02	0.25
G124-26	0.1469	12.39	0.33	-0.17	12.22	0.34
G200-39	0.2047	11.35	0.48	-0.35	11.00	0.53
GD337	0.8144	9.39	2.59	-3.59	5.80	24.43
L1126-68	0.6690	9.19	1.81	-2.00	7.19	18.00
G166-58	0.1257	12.96	0.31	-0.14	12.82	0.32
GD175	0.0953	13.86	0.31	-0.07	13.79	0.31
GD178	0.1711	10.82	0.44	-0.14	10.68	0.45
LP68-60	0.2230	12.76	0.91	-1.07	11.69	1.42
R808	0.1012	12.20	0.28	-0.11	12.09	0.29
G138-8	0.0649	13.90	0.19	-0.05	13.85	0.19
LP444-31	0.2327	11.71	0.59	-0.31	11.40	0.62
G138-31	0.0800	14.47	0.28	-0.12	14.35	0.29
R640	0.0613	12.78	0.18	-0.04	12.74	0.18
LP101-16	0.0597	13.99	0.21	-0.07	13.92	0.21
G180-63	0.0559	13.95	0.10	-0.01	13.94	0.10
G138-47	0.1435	13.98	0.38	-0.17	13.81	0.39
L1491-27	0.1095	12.33	0.25	-0.09	12.24	0.25
G138-56	0.4929	10.01	2.99	-2.20	7.81	118.97
GD358	0.1338	10.89	0.27	-0.05	10.84	0.27
G226-29	0.0453	11.83	0.13	-0.02	11.81	0.13
G169-34	0.0861	12.23	0.16	-0.04	12.19	0.16
G139-13	0.0653	13.97	0.21	-0.06	13.91	0.21
A+69 6829	0.0937	11.27	0.24	-0.09	11.18	0.24
W672A	0.1529	11.31	0.37	-0.22	11.09	0.39
G140-2	0.1581	12.74	0.36	-0.15	12.59	0.37
LP44-113	0.0226	15.25	0.05	0.00	15.25	0.05

Table 4. Continued

Star	Epsilon	Mv (uncorr)	±	Correction	Mv (Corr)	±
LP9-231	0.0633	13.15	0.18	-0.05	13.10	0.18
G206-18	0.1882	13.74	0.86	-0.01	13.73	0.10
G206-17	0.1882	12.89	0.58	-0.43	12.46	0.65
L1208132	0.1523	12.81	0.49	-0.29	12.52	0.52
LP103-294	0.0477	15.13	0.12	-0.02	15.11	0.12
R137	0.2497	9.81	0.48	-0.35	9.46	0.53
L993-18	0.1058	12.32	0.24	-0.06	12.26	0.24
G227-35	0.0557	14.64	0.13	-0.02	14.62	0.13
G184-12	0.2003	12.81	0.56	-0.52	12.29	0.68
GD215	0.0930	12.95	0.19	-0.03	12.92	0.19
L922-82	0.1046	11.97	0.24	-0.05	11.92	0.24
L1498-12	0.1216	12.06	0.31	-0.15	11.91	0.32
G125-3	0.0437	14.24	0.10	-0.91	13.33	1.20
L923-21	0.0372	12.29	0.10	-0.01	12.28	0.10
G185-32	0.0669	11.71	0.12	-0.02	11.69	0.12
GD222	0.1287	10.91	0.18	-0.03	10.88	0.18
L1573-31	0.1801	11.11	0.30	-0.07	11.04	0.30
L1285-97	0.1554	10.90	0.25	-0.07	10.83	0.25
L997-21	0.0446	13.33	0.11	-0.01	13.32	0.11
LP754-16	0.0656	15.65	0.22	-0.07	15.58	0.22
GD229	0.1076	12.56	0.17	-0.02	12.54	0.17
G24-9	0.0941	13.73	0.27	-0.11	13.62	0.28
W1346	0.0544	10.70	0.12	-0.02	10.68	0.12
G187-8	0.0751	14.07	0.15	-0.03	14.04	0.15
VB11	0.0597	15.55	0.19	-0.05	15.50	0.19
L1504-14	0.1266	12.43	0.26	-0.10	12.33	0.27
G144-51	0.1424	13.50	0.37	-0.15	13.35	0.38
G187-16	0.1032	14.37	0.25	-0.10	14.27	0.26
G25-20	0.0901	14.26	0.20	-0.04	14.22	0.20
L1433-34	0.1182	12.19	0.26	-0.10	12.09	0.27
R198	0.1245	12.14	0.32	-0.12	12.02	0.33
G261-43	0.0865	10.96	0.19	-0.03	10.93	0.19
L1002-16	0.1608	11.56	0.30	-0.13	11.43	0.31
G261-45	0.1163	10.56	0.40	-0.25	10.31	0.43
G212-45	0.1249	13.44	0.46	-0.32	13.12	0.50
G126-18	0.1561	12.16	0.29	-0.09	12.07	0.29
G126-25	0.6459	10.41	4.65	-2.95	7.46	484.92
L1363-3	0.0501	12.61	0.11	-0.02	12.59	0.11
L930-80	0.2566	10.65	0.89	-1.01	9.64	1.33
G188-27	0.1305	11.97	0.23	-0.06	11.91	0.23

Table 4. Continued

Star	Epsilon	Mv (uncorr)	±	Correction	Mv (Corr)	±
G93-48	0.0916	10.79	0.15	-0.02	10.77	0.15
G18-34	0.0941	13.66	0.25	-0.09	13.57	0.25
G241-6	0.2548	11.48	0.65	-0.55	10.93	0.76
G28-13	0.3902	11.04	1.31	-1.82	9.22	3.84
G67-23	0.0708	12.99	0.17	-0.04	12.95	0.17
G128-7	0.0757	13.99	0.21	-0.06	13.93	0.21
G156-64	0.1492	13.47	0.60	-0.59	12.88	0.76
L935-50	0.0930	13.44	0.26	-0.10	13.34	0.27
G157-35	0.0956	14.26	0.33	-0.17	14.09	0.34
G29-38	0.0509	12.37	0.13	-0.02	12.35	0.13
L1440-18	0.1419	12.44	0.39	-0.24	12.20	0.42
L1512-34	0.0626	11.81	0.12	-0.01	11.80	0.12
G130-15	0.0797	14.08	0.19	-0.05	14.03	0.19
G171-27	0.0963	12.89	0.21	-0.07	12.82	0.21

Note. Distance moduli and distances calculated with the corrected absolute visual magnitude are listed in Table 5.

Table 5. Distance Moduli and Distances of White Dwarf Sample

Star	Mv (Corr)	±	V	±	Dist. Mod.	±	Distance (pc)
LP49-275	11.57	0.24	14.33	0.01	2.76	0.24	35.65
G217-37	14.14	0.06	14.36	0.00	0.22	0.06	11.07
W1	12.83	0.32	15.34	0.00	2.51	0.32	31.77
L795-44	5.00	91.79	14.88	0.01	9.88	91.79	946.24
L1011-71	12.67	0.39	15.61	0.03	2.94	0.39	38.73
L1011-92	12.41	0.14	14.06	0.00	1.65	0.14	21.38
W28	14.22	0.03	12.39	0.00	-1.83	0.03	4.31
G1-45	12.32	0.18	13.96	0.01	1.64	0.18	21.28
W1516	12.78	0.12	13.83	0.02	1.05	0.12	16.22
G133-8	14.43	0.39	17.10	0.02	2.67	0.39	34.20
W72	11.62	0.25	14.38	0.01	2.76	0.25	35.65
R548	10.06	0.32	14.16	0.02	4.10	0.32	66.07
L870-2	12.45	0.09	12.86	0.01	0.41	0.09	12.08
G72-31	11.97	0.34	14.80	0.02	2.83	0.34	36.81
LP768-500	11.15	17.70	17.66		6.51		200.45
OXF+25 6	10.66	0.23	13.23	0.02	2.57	0.23	32.66
G74-7	13.55	0.13	14.51	0.01	0.96	0.13	15.56
G134-22	14.74	0.18	16.19	0.01	1.45	0.18	19.50
LP710-47	14.79	0.13	15.76	0.01	0.97	0.13	15.63
Feige 24	7.90	0.48	12.42	0.01	4.52	0.48	80.17
G75-39	13.85	0.23	15.53	0.02	1.68	0.23	21.68
G174-14	15.23	0.07	15.32	0.01	0.09	0.07	10.42
G76-48	13.63	0.21	15.90	0.02	2.27	0.21	28.44
W219	13.81	0.16	15.18	0.02	1.37	0.16	18.79
G37-44	9.78	1.51	15.49	0.04	5.71	1.51	138.68
G7-16	14.60	0.15	15.87	0.02	1.27	0.15	17.95
LB1240	11.64	0.17	13.81	0.02	2.17	0.17	27.16
G38-29	10.68	0.78	15.59	0.06	4.91	0.78	95.94
STN2051B	13.74	0.04	12.44		-1.30		5.50
G39-27	14.66	0.12	15.79	0.01	1.13	0.12	16.83
L879-14	13.88	0.06	13.76	0.00	-0.12	0.06	9.46
G175-46	12.41	0.38	15.96	0.04	3.55	0.38	51.29
GD64	10.74	0.25	14.00	0.01	3.26	0.25	44.87
G191-B2B	8.43	0.26	11.78	0.03	3.35	0.26	46.77
LP777-1	14.24	0.19	15.97	0.01	1.73	0.19	22.18
G86-B1B	10.28	0.93	16.09	0.02	5.81	0.93	145.21
LP119-48	12.30	0.32	15.56	0.00	3.26	0.32	44.87
G98-18	7.24	54.71	16.43	0.06	9.19	54.71	688.65
G99-37	14.31	0.07	14.53	0.01	0.22	0.07	11.07
G102-39	11.05	0.99	15.92	0.02	4.87	0.99	94.19

Table 5. Continued

Star	Mv (Corr)	±	V	±	Dist. Mod.	±	Distance (pc)
HL4	15.40	0.07	14.45	0.01	-0.95	0.07	6.46
G99-47	14.57	0.07	14.10	0.02	-0.47	0.07	8.05
L1244-26	10.15	0.30	13.39	0.01	3.24	0.30	44.46
G105-30	14.53	0.21	16.37	0.00	1.84	0.21	23.33
G108-26	14.32	0.15	15.68	0.01	1.36	0.15	18.71
HE3	11.24	0.08	12.05	0.02	0.81	0.08	14.52
LP58-53	13.83	0.39	16.64	0.02	2.81	0.39	36.48
G108-42	13.22	0.31	16.22	0.10	3.00	0.33	39.81
G87-29	13.75	0.18	15.54	0.03	1.79	0.18	22.80
G107-70	14.41	0.07	14.64	0.01	0.23	0.07	11.12
L745-46A	13.25	0.06	13.04	0.00	-0.21	0.06	9.08
G90-28	13.29	0.33	16.07	0.00	2.78	0.33	35.97
G193-78	12.25	0.30	15.08	0.01	2.83	0.30	36.81
G111-54	12.42	0.27	15.56	0.00	3.14	0.27	42.46
G111-71	12.81	0.47	16.55	0.02	3.74	0.47	55.98
G51-16	13.96	0.19	15.73	0.01	1.77	0.19	22.59
G47-18	13.63	0.16	15.18	0.05	1.55	0.17	20.42
G195-19	13.80	0.06	13.85	0.00	0.05	0.06	10.23
G116-16	13.03	0.25	15.37	0.00	2.34	0.25	29.38
G117B15A	10.65	0.93	15.50	0.01	4.85	0.93	93.33
G161-36	11.40	0.32	14.76	0.02	3.36	0.32	46.99
G117-25	13.31	0.33	15.91	0.04	2.60	0.33	33.11
SA29-130	10.64	0.23	13.30	0.01	2.66	0.23	34.04
G195-42	13.40	0.18	15.20	0.01	1.80	0.18	22.91
G49-33	13.08	0.24	15.07	0.03	1.99	0.25	25.00
G260-15	12.66	0.10	13.20	0.02	0.54	0.10	12.82
G43-38	13.70	0.25	16.04	0.02	2.34	0.25	29.38
G53-38	12.01	0.43	15.37	0.01	3.36	0.43	46.99
G235-67	13.65	0.13	14.71	0.00	1.06	0.13	16.29
G44-32	13.18	0.35	16.52	0.02	3.34	0.35	46.56
LP93-21	11.83	2.85	17.94		6.11		166.72
L898-25	13.97	0.11	14.33	0.02	0.36	0.11	11.80
LB253	10.45	0.44	13.79	0.01	3.34	0.44	46.56
L971-14	12.30	0.45	15.40	0.05	3.10	0.45	41.69
R627	13.64	0.12	14.32	0.07	0.68	0.14	13.68
G122-31	11.71	0.84	16.39	0.03	4.68	0.85	86.30
G148-7	11.20	0.24	13.65	0.04	2.45	0.24	30.90
L1405-40	12.11	0.41	15.67	0.01	3.56	0.41	51.52
L1261-24	13.12	0.27	15.63	0.01	2.51	0.27	31.77
G197-47	14.20	0.21	15.79	0.01	1.59	0.21	20.80

Table 5. Continued

Star	Mv (Corr)	±	V	±	Dist. Mod.	±	Distance (pc)
C1	10.87	0.27	13.30	0.01	2.43	0.27	30.62
G148-B4B	13.81	0.20	17.00		3.19		43.45
G61-17	11.43	0.69	15.86	0.02	4.43	0.69	76.91
L1408-19	12.65	0.32	15.39	0.01	2.74	0.32	35.32
W457	14.65	0.15	15.77	0.02	1.12	0.15	16.75
H243	8.44	0.49	12.68	0.01	4.24	0.49	70.47
G199-71	13.61	0.48	16.70	0.03	3.09	0.48	41.50
W485A	11.34	0.12	12.31	0.01	0.97	0.12	15.63
G165-7	13.54	0.36	16.04	0.01	2.50	0.36	31.62
GD325	11.30	0.26	14.00	0.02	2.70	0.26	34.67
W489	15.01	0.09	14.63	0.05	-0.38	0.10	8.39
G63-54	13.58	0.17	15.08	0.05	1.50	0.18	19.95
LP380-5	15.03	0.09	15.64	0.00	0.61	0.09	13.24
L1484-18	11.02	0.25	13.97	0.01	2.95	0.25	38.90
G124-26	12.22	0.34	15.36	0.02	3.14	0.35	42.46
G200-39	11.00	0.53	15.04	0.02	4.04	0.53	64.27
GD337	5.80	24.43	16.09	0.01	10.29	24.43	1142.88
L1126-68	7.19	18.00	15.46	0.04	8.27	18.00	450.82
G166-58	12.82	0.32	15.59	0.04	2.77	0.32	35.81
GD175	13.79	0.31	15.89	0.01	2.10	0.31	26.30
GD178	10.68	0.45	14.12	0.01	3.44	0.45	48.75
LP68-60	11.69	1.42	16.63	0.02	4.94	1.42	97.27
R808	12.09	0.29	14.36		2.27		28.44
G138-8	13.85	0.19	15.09	0.01	1.24	0.19	17.70
LP444-31	11.40	0.62	15.67	0.02	4.27	0.62	71.45
G138-31	14.35	0.29	16.12	0.01	1.77	0.29	22.59
R640	12.74	0.18	13.85	0.01	1.11	0.18	16.67
LP101-16	13.92	0.21	15.00		1.08		16.44
G180-63	13.94	0.10	14.82	0.02	0.88	0.10	15.00
G138-47	13.81	0.39	16.90		3.09		41.50
L1491-27	12.24	0.25	14.66	0.01	2.42	0.25	30.48
G138-56	7.81	118.97	15.70	0.09	7.89	118.97	378.44
GD358	10.84	0.27	13.65		2.81		36.48
G226-29	11.81	0.13	12.24	0.01	0.43	0.13	12.19
G169-34	12.19	0.16	14.04	0.01	1.85	0.16	23.44
G139-13	13.91	0.21	15.17	0.04	1.26	0.22	17.86
A+696829	11.18	0.24	13.26		2.08		26.06
W672A	11.09	0.39	14.36	0.00	3.27	0.39	45.08
G140-2	12.59	0.37	15.86	0.02	3.27	0.37	45.08
LP44-113	15.25	0.05	14.15	0.01	-1.10	0.05	6.03

Table 5. Continued

Star	Mv (Corr)	±	V	±	Dist. Mod.	±	Distance (pc)
LP9-231	13.10	0.18	14.29	0.00	1.19	0.18	17.30
G206-18	13.73	0.10	17.24	0.21	3.51	0.23	50.35
G206-17	12.46	0.65	16.40	0.02	3.94	0.65	61.38
L1208132	12.52	0.52	15.86	0.06	3.34	0.53	46.56
LP103-394	15.11	0.12	15.65	0.02	0.54	0.12	12.82
R137	9.46	0.53	13.93	0.06	4.47	0.54	78.34
L993-18	12.26	0.24	14.57	0.01	2.31	0.24	28.97
G227-35	14.62	0.13	15.50	0.02	0.88	0.13	15.00
G184-12	12.29	0.68	16.45	0.02	4.16	0.68	67.92
GD215	12.92	0.19	14.92	0.03	2.00	0.19	25.12
L922-82	11.92	0.24	14.20	0.00	2.28	0.24	28.58
L1498-12	11.91	0.32	14.62	0.02	2.71	0.32	34.83
G125-3	13.33	1.20	14.58	0.04	1.25	1.20	17.78
L923-21	12.28	0.10	12.28	0.02	0.00	0.10	10.00
G185-32	11.69	0.12	12.97	0.01	1.28	0.12	18.03
GD222	10.88	0.18	13.59		2.71		34.83
L1573-31	11.04	0.30	14.52	0.01	3.48	0.30	49.66
L1285-97	10.83	0.25	13.99	0.00	3.16	0.25	42.85
L997-21	13.32	0.11	13.71	0.05	0.39	0.12	11.97
LP754-16	15.58	0.22	16.87	0.05	1.29	0.23	18.11
GD229	12.54	0.17	14.85	0.02	2.31	0.17	28.97
G24-9	13.62	0.28	15.73	0.02	2.11	0.28	26.42
W1346	10.68	0.12	11.51	0.00	0.83	0.12	14.66
G187-8	14.04	0.15	15.58	0.03	1.54	0.15	20.32
VB11	15.50	0.19	16.56	0.03	1.06	0.19	16.29
L1504-14	12.33	0.27	15.07	0.02	2.74	0.27	35.32
G144-51	13.35	0.38	16.40	0.05	3.05	0.38	40.74
G187-16	14.27	0.26	16.57	0.01	2.30	0.26	28.84
G25-20	14.22	0.20	16.17	0.02	1.95	0.20	24.55
L1433-34	12.09	0.27	14.69	0.01	2.60	0.27	33.11
R198	12.02	0.33	14.75	0.00	2.73	0.33	35.16
G261-43	10.93	0.19	12.78	0.02	1.85	0.19	23.44
L1002-16	11.43	0.31	14.73	0.01	3.30	0.31	45.71
G261-45	10.31	0.43	13.02	0.00	2.71	0.43	34.83
G212-45	13.12	0.50	16.05	0.12	2.93	0.52	38.55
G126-18	12.07	0.29	15.25	0.04	3.18	0.30	43.25
G126-25	7.46	484.92	16.58	0.02	9.12	484.92	666.81
L1363-3	12.59	0.11	13.24	0.02	0.65	0.11	13.49
L930-80	9.64	1.33	14.83	0.03	5.19	1.33	109.14
G188-27	11.91	0.23	14.68	0.02	2.77	0.23	35.81

Table 5. Continued

Star	Mv (Corr)	±	V	±	Dist. Mod.	±	Distance (pc)
G93-48	10.77	0.15	12.73	0.03	1.96	0.15	24.66
G18-34	13.57	0.25	15.66	0.03	2.09	0.26	26.18
G241-6	10.93	0.76	15.65	0.01	4.72	0.76	87.90
G28-13	9.22	3.84	16.14	0.04	6.92	3.84	242.10
G67-23	12.95	0.17	14.37	0.01	1.42	0.17	19.23
G128-7	13.93	0.21	15.52	0.01	1.59	0.21	20.80
G156-64	12.88	0.76	16.47	0.01	3.59	0.76	52.24
L935-50	13.34	0.27	15.42	0.01	2.08	0.27	26.06
G157-35	14.09	0.34	16.29	0.02	2.20	0.34	27.54
G29-38	12.35	0.13	13.03	0.02	0.68	0.13	13.68
L1440-18	12.20	0.42	15.33	0.02	3.13	0.42	42.27
L1512-34	11.80	0.12	12.93	0.01	1.13	0.12	16.83
G130-15	14.03	0.19	15.72	0.01	1.69	0.19	21.78
G171-27	12.82	0.21	14.94	0.01	2.12	0.21	26.55

Table 6. Stars Excluded Because of Large Relative Parallax Error

Star	ε-value	Corrected Mv	Uncertainty
GD337	1.1739	5.80	+ 24.43
G28-13	0.5938	9.22	3.84
L795-44	1.4103	5.00	91.79
LP68-60	0.4167	11.69	1.42
G206-18	0.3819	12.83	1.20
G102-39	0.3510	11.05	0.99
L930-80	0.4041	9.64	1.33
G126-25	2.1552	7.46	484.92
G37-44	0.3793	9.78	1.51
G98-18	1.0769	7.24	54.71
G138-56	1.3158	7.81	118.97
L1126-68	0.8036	7.39	18.00
LP768-500	0.8000	11.15	17.70
LP93-21	0.3286	12.41	1.30

Table 7. Temperature and Gravity Data for Stars in the White Dwarf Sample

Star	Teff (*1000)	± (*1000)	log(Teff)	±	log g	±
LP49-275	22.08	0.98	4.34	0.02	7.83	0.44
W1	10.00	1.00	4.00	0.04	7.86	0.20
L1011-71	11.31	1.40	4.05	0.05	8.60	0.20
L1011-92	17.71	0.60	4.25	0.01	8.35	0.22
G1-45	7.50	0.26	3.88	0.02	8.20	1.00
W72	8.15	0.56	3.91	0.03	7.39	0.26
R548	11.80	0.60	4.07	0.02	7.75	0.18
G72-31	11.70	1.40	4.07	0.05	8.00	0.20
OXF+25 6	19.88	0.72	4.30	0.02	7.75	0.30
Feige 24	26.00	0.98	4.41	0.02	8.00	0.44
LB1240	13.76	0.46	4.14	0.01	7.80	0.22
G38-29	8.88	0.56	3.95	0.03	7.68	0.26
G175-46	10.00	1.00	4.00	0.04	8.27	0.30
GD64	15.07	0.72	4.18	0.02	7.70	0.30
G86-B1B	8.20	0.25	3.91	0.01	8.28	0.25
LP119-48	21.10	0.98	4.32	0.02	8.95	0.44
G108-26	7.10	0.32	3.85	0.02	7.40	0.48
HE3	22.93	0.98	4.36	0.02	7.60	0.44
G108-42	15.79	0.60	4.20	0.02	8.20	0.22
L745-46A	8.73	0.50	3.94	0.02	8.22	0.50
G111-71	8.13	0.56	3.91	0.03	7.60	0.26
G51-16	7.70	0.32	3.89	0.02	7.48	0.48
G116-16	10.50	1.00	4.02	0.04	8.07	0.40
G117-B15A	13.00	1.40	4.11	0.05	8.24	0.20
G161-36	13.86	0.46	4.14	0.01	7.85	0.22
G117-25	9.00	0.56	3.95	0.03	7.95	0.26
SA29-130	12.45	0.60	4.10	0.02	7.43	0.18
G49-33	8.73	0.56	3.94	0.03	7.36	0.26
G260-15	18.50	0.60	4.27	0.01	8.57	0.22
G53-38	8.16	0.56	3.91	0.03	7.00	0.26
G44-32	7.50	0.26	3.88	0.02	8.50	1.00
L898-25	7.33	0.32	3.87	0.02	7.53	0.48
LB253	18.69	0.72	4.27	0.02	7.60	0.30
L971-14	17.00	0.60	4.23	0.02	8.03	0.22
R627	8.16	0.56	3.91	0.03	7.00	0.26
G122-31	20.00	0.60	4.30	0.01	[illegible]	0.22
G148-7	16.13	0.72	4.21	0.02	7.75	0.30
L1405-40	11.00	1.00	4.04	0.04	8.28	0.40
G61-17	11.00	1.00	4.04	0.04	7.99	0.40
L1408-19	8.50	0.50	3.93	0.03	8.15	0.50

Table 7. Continued

Star	Teff (*1000)	± (*1000)	log(Teff)	±	log g	±
W485A	14.68	0.46	4.17	0.01	7.80	0.22
GD325	20.13	0.98	4.30	0.02	8.87	0.44
L1484-18	18.25	0.72	4.26	0.02	7.60	0.30
G200-39	23.50	0.98	4.37	0.02	8.30	0.44
GD178	15.13	0.72	4.18	0.02	7.60	0.30
R808	12.47	0.60	4.10	0.02	7.93	0.18
G138-8	9.00	0.50	3.95	0.02	8.20	0.50
LP444-31	15.06	0.72	4.18	0.02	7.70	0.30
L1491-27	12.20	1.40	4.09	0.05	8.02	0.20
G226-29	13.40	0.46	4.13	0.01	7.19	0.22
G169-34	8.19	0.56	3.91	0.03	7.20	0.26
A+69 6829	16.25	0.72	4.21	0.02	7.80	0.30
W672A	13.97	0.46	4.15	0.01	7.73	0.22
L933-18	8.70	0.50	3.94	0.02	8.00	0.50
G184-12	8.20	0.56	3.91	0.03	7.80	0.26
GD215	13.51	0.46	4.13	0.01	7.96	0.22
L1498-12	13.30	0.46	4.12	0.02	7.23	0.22
L923-21	17.46	0.60	4.24	0.01	8.50	0.22
G185-32	12.50	0.60	4.10	0.02	7.93	0.18
GD222	22.18	0.98	4.35	0.02	7.60	0.44
L1285-97	19.25	0.72	4.28	0.02	7.65	0.30
W1346	21.25	0.98	4.33	0.02	7.55	0.44
L1504-14	16.33	0.60	4.21	0.02	8.60	0.22
L1433-34	8.40	0.50	3.92	0.03	8.53	0.50
R198	14.60	0.70	4.16	0.02	8.30	0.20
G261-43	16.25	0.72	4.21	0.02	7.40	0.30
G261-45	17.50	0.72	4.24	0.02	7.50	0.30
G126-18	12.53	0.60	4.10	0.02	7.54	0.18
G93-48	17.14	0.60	4.23	0.02	8.22	0.22
G18-34	8.85	0.56	3.95	0.03	7.65	0.26
G241-6	22.30	0.98	4.35	0.02	8.25	0.44
G67-23	13.19	0.70	4.12	0.02	8.44	0.20
L935-50	9.50	1.00	3.98	0.05	8.38	0.30
G29-38	13.88	0.70	4.14	0.02	8.20	0.20
L1440-18	12.07	1.40	4.08	0.05	8.36	0.20
L1512-34	13.74	0.70	4.14	0.02	8.04	0.20

It is useful to compare these results with those of other researchers. Bergeron et al. (1992) have published estimates of T_{eff} and log g for many of our stars as derived from model atmosphere fitting (see table 8).

Table 8. Comparison of T_{eff}, log g Data Between This Paper and Bergeron et al. (1992)

	This Paper				Bergeron et al.			
star	Teff	±	log g	±	Teff	log g	ΔTeff	Δlog g
GD 64	15070	720	7.70	0.30	14260	7.71	-810	0.01
He 3	22930	980	7.60	0.44	21060	8.10	-1870	0.50
LB 253	18690	720	7.60	0.30	18220	8.04	-470	0.44
G148-7	16130	720	7.75	0.30	15360	7.99	-770	0.24
W485A	14680	460	7.80	0.22	14350	7.92	-330	0.12
L1484-18	18250	720	7.60	0.30	18410	7.97	160	0.37
GD 178	15130	720	7.60	0.30	14660	8.00	-470	0.40
GD 222	22180	980	7.60	0.44	21260	7.84	-920	0.24
W1346	21250	980	7.55	0.44	19980	7.83	-1270	0.28
G261-45	17500	720	7.50	0.30	16940	7.84	-560	0.34
G93-48	17140	600	8.22	0.22	18250	8.02	1110	-0.20

Table 9. Theoretical Bolometric Correction–Temperature Data from Model Atmospheres for DA White Dwarfs

Shipman		Wesemael et al.	
T_{eff}(K)	B.C.	T_{eff}(K)	B.C.
5000	–0.39	20000	–2.012
6000	–0.29	22500	–2.32
7000	–0.35	27500	–2.82
8000	–0.41	30000	–3.013
9000	–0.47	32500	–3.17
10000	–0.53	35000	–3.34
12000	–0.82	40000	–3.787
14000	–1.21	45000	–4.17
20000	–2.14	50000	–4.516
		60000	–5.15
		70000	–5.691
		90000	–6.56

Note. The corrections from Wesemael et al. are calculated for log g =8, the corrections from Shipman neglect convection.

Table 10. Mv, Bolometric Correction, and M_{bol} for Stars in the White Dwarf Sample

Star	Mv	±	Bolometric Correction	±	M_{bol}	±
LP49-275	11.57	0.24	-2.14	0.04	9.43	0.24
W1	12.83	0.32	-0.64	0.02	12.19	0.32
L1011-71	12.67	0.39	-0.79	0.04	11.88	0.39
L1011-92	12.41	0.14	-1.65	0.01	10.76	0.14
G1-45	12.32	0.18	-0.38	0.01	11.94	0.18
W72	11.62	0.25	-0.43	0.01	11.19	0.25
R548	10.06	0.32	-0.86	0.02	9.20	0.32
G72-31	11.97	0.34	-0.86	0.04	11.11	0.34
OXF+25 6	10.66	0.23	-1.91	0.03	8.75	0.23
Feige 24	7.90	0.48	-2.55	0.04	5.35	0.48
LB1240	11.64	0.17	-1.13	0.01	10.51	0.17
G38-29	10.68	0.78	-0.51	0.01	10.17	0.78
G175-46	12.41	0.38	-0.64	0.02	11.77	0.38
GD64	10.74	0.25	-1.31	0.02	9.43	0.25
G86-B1B	10.28	0.93	-0.43	0.00	9.85	0.93
LP119-48	12.30	0.32	-2.02	0.03	10.28	0.32
G108-26	14.32	0.15	-0.34	0.01	13.98	0.15
HE3	11.24	0.08	-2.21	0.04	9.04	0.09
G108-42	13.22	0.31	-1.40	0.02	11.82	0.31
L745-46A	13.25	0.06	-0.49	0.01	12.76	0.06
G111-71	12.81	0.47	-0.43	0.01	12.38	0.47
G51-16	13.96	0.19	-0.39	0.01	13.57	0.19
G116-16	13.03	0.25	-0.70	0.03	12.33	0.25
G117-B15A	10.65	0.93	-1.01	0.05	9.64	0.93
G161-36	11.40	0.32	-1.13	0.01	10.27	0.32
G117-25	13.31	0.33	-0.51	0.01	12.80	0.33
SA29-130	10.64	0.23	-0.97	0.02	9.67	0.23
G49-33	13.08	0.24	-0.49	0.01	12.59	0.24
G260-15	12.66	0.10	-1.75	0.02	10.91	0.10
G53-38	12.01	0.43	-0.43	0.01	11.58	0.43
G44-32	13.18	0.35	-0.38	0.01	12.80	0.35
L898-25	13.97	0.11	-0.36	0.01	13.61	0.11
LB253	10.45	0.44	-1.75	0.03	8.70	0.44
L971-14	12.30	0.45	-1.55	0.03	10.75	0.45
R627	13.64	0.12	-0.43	0.01	13.21	0.12
G122-31	11.71	0.84	-1.91	0.02	9.80	0.84
G148-7	11.20	0.24	-1.45	0.03	9.75	0.24
L1405-40	12.11	0.41	-0.76	0.03	11.35	0.41
G61-17	11.43	0.69	-0.76	0.03	10.67	0.69
L1408-19	12.65	0.32	-0.47	0.01	12.18	0.32

Table 10. Continued

Star	Mv	±	Bolometric Correction	±	M_{bol}	±
W485A	11.34	0.12	-1.26	0.01	10.08	0.12
GD325	11.30	0.26	-1.91	0.03	9.39	0.26
L1484-18	11.02	0.25	-1.70	0.03	9.32	0.25
G200-39	11.00	0.53	-2.31	0.04	8.69	0.53
GD178	10.68	0.45	-1.31	0.02	9.37	0.45
R808	12.09	0.29	-0.97	0.02	11.12	0.29
G138-8	13.85	0.19	-0.51	0.01	13.34	0.19
LP444-31	11.40	0.62	-1.31	0.02	10.09	0.62
L1491-27	12.24	0.25	-0.94	0.04	11.30	0.25
G226-29	11.81	0.13	-1.09	0.01	10.72	0.13
G169-34	12.19	0.16	-0.43	0.01	11.76	0.16
A+69 6829	11.18	0.24	-1.45	0.03	9.73	0.24
W672A	11.09	0.39	-1.18	0.01	9.91	0.39
L993-18	12.26	0.24	-0.49	0.01	11.77	0.24
G184-12	12.29	0.68	-0.43	0.01	11.86	0.68
GD215	12.92	0.19	-1.09	0.01	11.83	0.19
L1498-12	11.91	0.32	-1.05	0.02	10.86	0.32
L923-21	12.28	0.10	-1.60	0.01	10.68	0.10
G185-32	11.69	0.12	-0.97	0.02	10.72	0.12
GD222	10.88	0.18	-2.19	0.04	8.69	0.18
L1285-97	10.83	0.25	-1.80	0.03	9.03	0.25
W1346	10.68	0.12	-2.08	0.04	8.60	0.13
L1504-14	12.33	0.27	-1.45	0.03	10.88	0.27
L1433-34	12.09	0.27	-0.45	0.01	11.64	0.27
R198	12.02	0.33	-1.22	0.02	10.80	0.33
G261-43	10.93	0.19	-1.45	0.03	9.48	0.19
G261-45	10.31	0.43	-1.60	0.03	8.71	0.43
G126-18	12.07	0.29	-0.97	0.02	11.10	0.29
G93-48	10.77	0.15	-1.55	0.03	9.22	0.15
G18-34	13.57	0.25	-0.51	0.01	13.06	0.25
G241-6	10.93	0.76	-2.19	0.04	8.74	0.76
G67-23	12.95	0.17	-1.05	0.02	11.90	0.17
L935-50	13.34	0.27	-0.58	0.03	12.76	0.27
G29-38	12.35	0.13	-1.13	0.02	11.22	0.13
L1440-18	12.20	0.42	-0.90	0.04	11.30	0.42
L1512-34	11.80	0.12	-1.13	0.02	10.67	0.12

Table 11. Log Radii and Masses of White Dwarf Sample

Star	$\log\left(\frac{R_*}{R_\odot}\right)$	M_* (in $M_\odot$)
L1512-34	-2.10	0.15
W1	-1.97	0.30
L1011-71	-2.01	1.38
L1011-92	-2.18	0.35
G72-31	-1.89	0.60
OXF+25 6	-1.87	0.37
LB1240	-1.91	0.35
G175-46	-1.88	1.17
GD64	-1.77	0.52
LP119-48	-2.23	1.12
H: 3	-2.06	0.11
G116-16	-2.04	0.35
G117-B15A	-1.68	2.75
G161-36	-1.87	0.47
SA29-130	-1.65	0.49
G260-15	-2.24	0.45
LB253	-1.81	0.35
L971-14	-2.14	0.20
G122-31	-2.09	1.51
G148-7	-1.89	0.34
L1405-40	-1.88	1.20
G61-17	-1.74	1.17
W485A	-1.88	0.40
GD325	-2.01	2.57
L1484-18	-1.91	0.22
G200-39	-2.01	0.69
GD178	-1.76	0.44
R808	-1.94	0.41
LP444-31	-1.90	0.29
L1491-27	-1.96	0.46
G226-29	-1.93	0.08
A+ 69 6829	-1.90	0.36
W672A	-1.80	0.49
GD215	-2.16	0.16
L1498-12	-1.95	0.08
L923-21	-2.15	0.58
G185-32	-1.87	0.56
GD222	-1.96	0.17
L1285-97	-1.90	0.26
W1346	-1.90	0.20

Table 11. Continued

Star	$\log\left(\frac{R_*}{R_\odot}\right)$	M_* (in $M_\odot$)
L1504–14	–2.13	0.79
R198	–2.02	0.66
G261–43	–1.85	0.18
G261–45	–1.76	0.35
G126–18	–1.94	0.17
G93–48	–1.84	1.26
G241–6	–1.97	0.74
G67–23	–2.15	0.50
L935–50	–2.04	0.75
G29–38	–2.06	0.44
L1440–18	–1.95	1.05
L1512–34	–1.94	0.52

Table 12. Stellar Distances From UBV Photometry

Stars	V	±	Dist.Mod. (true)	±	log g	ΔM_{bol^*}	${}^{R}M_{bol^*}$
LP49-275	14.33	0.01	2.76	0.24	7.83	-0.98	8.45
W1	15.34	0.00	2.51	0.32	7.86	-0.30	11.89
L1011-71	15.16	0.03	2.94	0.39	8.60	-0.53	11.35
L1011-92	14.06	0.00	1.65	0.14	8.35	-1.36	9.40
G72-31	14.80	0.02	2.83	0.34	8.00	0.09	11.20
OXF+25 6	13.23	0.02	2.57	0.23	7.75	0.15	8.90
LB 1240	13.81	0.02	2.17	0.17	7.80	-0.01	10.50
G175-46	15.96	0.04	3.55	0.38	8.27	0.12	11.89
GD64	14.00	0.01	3.26	0.25	7.70	0.67	10.10
LP119-48	15.56	0.00	3.26	0.32	8.95	-1.64	8.64
HE3	12.05	0.02	0.81	0.08	7.60	-0.76	8.28
G116-16	15.37	0.00	2.34	0.25	8.07	-0.66	11.67
G117B15A	15.50	0.01	4.85	0.93	8.24	1.11	10.75
G161-36	14.76	0.02	3.36	0.32	7.85	0.20	10.47
SA29-130	13.30	0.01	2.66	0.23	7.43	1.26	10.93
G260-15	13.20	0.02	0.54	0.10	8.57	-1.70	9.21
LB253	13.79	0.01	3.34	0.44	7.60	0.47	9.17
L971-14	15.40	0.05	3.10	0.45	8.03	-1.17	9.58
G122-31	16.39	0.03	4.68	0.85	8.80	-0.92	8.88
G148-7	13.65	0.04	2.45	0.24	7.75	0.06	9.81
L1405-40	15.67	0.01	3.56	0.41	8.28	0.12	11.47
G61-17	15.86	0.02	4.43	0.69	7.99	0.80	11.47
W485A	12.31	0.01	0.97	0.12	7.80	0.14	10.22
GD325	14.00	0.02	2.70	0.26	8.87	-0.54	8.85
L1484-18	13.97	0.01	2.95	0.25	7.60	-0.05	9.27
G200-39	15.04	0.02	4.04	0.53	8.30	-0.51	8.18
GD178	14.12	0.01	3.44	0.45	7.60	0.72	10.09
R808	14.36		2.27		7.93	-0.19	10.93
LP444-31	15.67	0.02	4.27	0.62	7.70	0.02	10.11
L1491-27	14.66	0.01	2.42	0.25	8.02	-0.28	11.02
G226-29	12.24	0.01	0.43	0.13	7.19	-0.11	10.61
A+69 6829	13.26		2.08		7.80	0.05	9.78
W672A	14.36	0.00	3.27	0.39	7.73	0.52	10.43
GD215	14.92	0.03	2.00	0.19	7.96	-1.25	10.58
L1498-12	14.62	0.02	2.71	0.32	7.23	-0.21	10.65
L923-21	12.28	0.02	0.00	0.10	8.50	-1.21	9.47
G185-32	12.97	0.01	1.28	0.12	7.93	0.20	10.92
GD222	13.59		2.71		7.60	-0.26	8.43
L1285-97	13.99	0.00	3.16	0.25	7.65	0.01	9.04
W1346	11.51	0.00	0.83	0.12	7.55	0.01	8.61

Table 12. Continued

Stars	V	±	V–Mv (true)	±	log g	ΔM_{bol}*	${}^{R}M_{bol}$*
L1504–14	15.07	0.02	2.74	0.27	8.60	–1.12	9.76
R198	14.75	0.00	2.73	0.33	8.30	–0.56	10.24
G261–43	12.78	0.02	1.85	0.19	7.40	0.30	9.78
G261–45	13.02	0.00	2.71	0.43	7.50	0.75	9.46
G126–18	15.25	0.04	3.18	0.30	7.54	–0.19	10.91
G93–48	12.73	0.03	1.96	0.15	8.22	0.33	9.55
G241–6	15.65	0.01	4.72	0.76	8.25	–0.34	8.40
G67–23	14.37	0.01	1.42	0.17	8.44	–1.22	10.68
L935–50	15.42	0.01	2.08	0.27	8.38	–0.65	12.11
G29–38	13.03	0.02	0.68	0.13	8.20	–0.76	10.46
L1440–18	15.33	0.02	3.13	0.42	8.36	–0.23	11.07
L1512–34	12.93	0.01	1.13	0.12	8.04	–0.16	10.51

Table 13. Comparison of Distance Moduli

Star	M_{bol}* ('new')	B.C.	Mv ('new')	dist. mod. ('new')	d.mod. 'new'–true
LP49-275	8.52	-2.14	10.66	3.67	0.91
W1	11.99	-0.64	12.63	2.71	0.20
L1011-71	12.15	-0.79	12.94	2.67	-0.27
L1011-92	9.97	-1.65	11.62	2.44	0.79
G72-31	11.44	-0.86	12.30	2.50	-0.33
OXF+25 6	8.90	-1.91	10.81	2.42	-0.15
LB 1240	10.55	-1.13	11.68	2.13	-0.04
G175-46	12.37	-0.64	13.01	2.95	-0.60
GD64	10.06	-1.31	11.37	2.63	-0.63
LP119-48	9.76	-2.02	11.78	3.78	0.52
HE3	8.14	-2.21	10.34	1.71	0.90
G116-16	11.97	-0.70	12.67	2.70	0.36
G117B15A	11.21	-1.01	12.22	3.28	-1.57
G161-36	10.56	-1.13	11.69	3.07	-0.29
SA29-130	10.64	-0.97	11.61	1.69	-0.97
G260-15	9.98	-1.75	11.73	1.47	0.93
LB253	9.03	-1.75	10.78	3.01	-0.33
L971-14	9.84	-1.65	11.39	4.01	0.91
G122-31	9.86	-1.91	11.77	4.62	-0.06
G148-7	9.81	-1.45	11.26	2.39	-0.06
L1405-40	11.97	-0.76	12.73	2.94	-0.62
G61-17	11.70	-0.76	12.46	3.40	-1.03
W485A	10.27	-1.26	11.53	0.78	-0.19
GD325	9.89	-1.91	11.80	2.20	-0.50
L1464-18	9.14	-1.70	10.84	3.13	0.18
G200-39	8.69	-2.31	11.00	4.04	0.00
GD178	9.95	-1.31	11.26	2.86	-0.58
R808	11.10	-0.97	12.07	2.29	0.02
LP444-31	10.06	-1.31	11.37	4.30	0.03
L1491-27	11.28	-0.94	12.22	2.44	0.02
G226-29	10.09	-1.09	11.18	1.06	0.63
A+69 6829	9.83	-1.45	11.28	1.98	-0.10
W672A	10.42	-1.18	11.60	2.76	-0.51
GD215	10.78	-1.09	11.87	3.05	1.05
L1498-12	10.16	-1.05	11.21	3.41	0.70
L923-21	10.17	-1.60	11.77	0.51	0.51
G185-32	11.09	-0.97	12.06	0.91	-0.37
GD222	8.29	-2.19	10.48	3.11	0.40
L1285-97	8.95	-1.80	10.75	3.24	0.08
W1346	8.43	-2.08	10.51	1.00	0.17

Table 13. Continued

Star	M_{bol}* ('new')	B.C.	M_V ('new')	dist. mod. ('new')	d.mod. 'new'–true
L1504–14	10.55	–1.45	12.00	3.07	0.33
R198	10.76	–1.22	11.98	2.77	0.04
G261–43	9.45	–1.45	10.90	1.88	0.03
G261–45	9.22	–1.60	10.82	2.20	–0.51
G126–18	10.71	–0.97	11.69	3.56	0.38
G93–48	9.99	–1.55	11.54	1.19	0.77
G241–6	8.87	–2.19	11.06	4.59	0.13
G67–23	11.33	–1.05	12.38	1.99	0.57
L935–50	12.70	–0.58	13.28	2.14	0.06
G29–38	10.88	–1.13	12.01	1.02	0.34
L1440–18	11.64	–0.90	12.54	2.79	–0.34
L1512–34	10.78	–1.13	11.91	1.02	0.11

Table 14. Photometric Distances of Hyades Stars From Agayev (1982)

Star	log Teff	log g	M_{bol}*	B.C.	Mv	V–Mv
77	4.14	8.35	11.07	–1.13	12.20	2.27
80	4.17	7.95	10.40	–1.26	11.66	3.49
90	4.29	7.92	9.17	–1.86	11.03	3.26
95	4.31	8.13	9.17	–1.97	11.14	3.04
100	4.44	7.56	7.96	–2.74	10.70	3.12

Curriculum Vitae

Name: Jeremy Robert Wilson Beckett
Birthplace: Montreal, Quebec
Birthdate: 12 September, 1966

Education: Concordia University,
Montreal, Quebec,
B.Sc. Physics, 1989

Saint Mary's University,
Halifax, Nova Scotia,
M.Sc. Astronomy, 1994
"Empirical Confirmation of the Mass Dependence for White Dwarf Luminosities"

Dalhousie University,
Halifax, Nova Scotia,
B.Sc. Physics, 1994 (Upgrading)

Experience: Observatory Demonstrator,
Department of Astronomy,
Saint Mary's University,
1989--1991

Presented Papers: "Empirical Confirmation of the Mass Dependence for White Dwarf Luminosities",
Jeremy R.W. Beckett and David G. Turner, poster display, 23rd Annual Meeting of the Canadian Astronomical Society,
Halifax, Nova Scotia, 1992